THE EUROPEAN
PHYSICAL JOURNAL C

CrossMark

A systematic study of mass spectra and strong decay of strange mesons

Cheng-Qun Pang[1,2], **Jun-Zhang Wang**[1,3], **Xiang Liu**[1,3,a] , **Takayuki Matsuki**[4,5,b]

[1] School of Physical Science and Technology, Lanzhou University, Lanzhou 730000, China
[2] College of Physics and Electronic Information Engineering, Qinghai Normal University, Xining 810000, China
[3] Research Center for Hadron and CSR Physics, Lanzhou University and Institute of Modern Physics of CAS, Lanzhou 730000, China
[4] Tokyo Kasei University, 1-18-1 Kaga, Itabashi, Tokyo 173-8602, Japan
[5] Theoretical Research Division, Nishina Center, RIKEN, Saitama 351-0198, Japan

Abstract The mass spectrum of the kaon family is analyzed by the modified Godfrey–Isgur model with a color screening effect approximating the kaon as a heavy–light meson system. This analysis gives us the structure and possible assignments of the observed kaon candidates, which can be tested by comparing the theoretical results of their two-body strong decays with the experimental data. Additionally, prediction of some partial decay widths is made on the kaons still missing in experiment. This study is crucial to establishing the kaon family and searching for their higher excitations in the future.

1 Introduction

As an important part of the meson family, the kaon subfamily has become more and more abundant with experimental progress on the observations of the kaons in the past decades. Until now, the Particle Data Group (PDG) has collected dozens of the kaons [1]. When facing so abundantly many kaons, it is one of the main tasks of the present study of light hadron spectroscopy to categorize them into the family and another task is to investigate the higher radial and orbital excitations.

Before the present work, there were some theoretical papers related to kaons. For example, 30 years ago, Godfrey and Isgur [2] developed a relativistic quark model, the so-called Godfrey–Isgur (GI) model, by which they studied the mass spectrum of hadrons including kaons. In 2002, Barnes et al. [3] further investigated the strong decays of the observed kaons, which have masses less than 2.2 GeV, where the $^3P_0$

quark model associated with a simple harmonic oscillator (SHO) wave function was adopted in their calculation. In 2009, Ebert et al. [4] analyzed the mass spectrum and Regge trajectories of the kaons by their relativistic quark model.

Due to the present experimental progress on kaons, it is a suitable time to systematically carry out phenomenological study of the kaons. In this work, we first calculate the mass spectra of the kaon family by applying the modified GI model [5,6], where the screening effect is taken into account. Fitting some well-established kaon states, we fix the parameters in the model, which are adopted when calculating the masses of other kaon states. Comparing theoretical results with experimental data, we obtain the structure information of the discussed kaons. Especially, we predict some radial ground states of the kaon which are still missing in experiments, e.g. $K_4(2310)(1^1G_4)$. Using our potential model approach, the spatial wave functions of the kaons studied can be numerically calculated, which we take as input when studying their Okubo–Zweig–Iizuka (OZI)-allowed two-body strong decays. For further testing the properties of the kaons, we study their OZI-allowed two-body strong decays, which provide valuable information of their partial and total decay widths, where one uses the quark pair creation (QPC) model which was proposed in Ref. [7] and extensively applied to studies of other hadrons in Refs. [8–34]. Analyzing mass spectra and calculating strong decay behaviors, we finally identify their $n^{2S+1}L_J$ quantum numbers, which reflect the inner structure of the kaons under discussion. Here, we predict the strong decay behaviors of some kaon states, e.g. $K_4(2310)(1^1G_4)$ has a wide width about 710–880 MeV, and mainly decays into $K_4^*(2045)\pi$, $K_3^*(1780)\pi$, $K\rho_3(1690)$ and Ka_2. The study presented in this work is helpful for establishing the kaon family by including higher radial and orbital excitations.

[a] e-mail: xiangliu@lzu.edu.cn

[b] e-mail: matsuki@tokyo-kasei.ac.jp

Springer

This paper is organized as follows. After Introduction, in Sect. 2 we explain the modified Godfrey–Isgur model and the QPC model. In Sect. 3, we adopt the modified Godfrey–Isgur model by including the screening effect to study the mass spectra of the kaon family. Making a comparison between theoretical and experimental results, we further obtain the structure information of the observed kaons. In Sect. 4, we present the detailed study of the OZI-allowed two-body strong decays of the discussed kaons. The paper ends with conclusions and discussion.

2 Phenomenological quark models adopted in this work

In our calculation, two phenomenological quark models are adopted, i.e., the modified GI model with the color screening effect[1] and the QPC model. The modified GI quark model is applied to calculate the mass spectrum of the kaon family, by which we obtain the structure information of the observed kaon candidates. Then we further test the possible assignments by comparing the theoretical results of their two-body OZI-allowed decays with the experimental data, where the QPC model is used to calculate their strong decays.

In the following, we will introduce these two models.

2.1 The modified GI model

First, we introduce the Godfrey–Isgur (GI) relativized quark model and discuss how the GI model is modified by including the color screening effect. Below we describe the detailed procedure and equations actually done by us because those are necessary in our work but are not familiar to the general reader. Some are common to Godfrey and Isgur.

The interaction between quark and antiquark in the GI model [2] is described by the Hamiltonian

$$\tilde{H} = \left(p^2 + m_{u/d}^2 \right)^{1/2} + \left(p^2 + m_s^2 \right)^{1/2} + \tilde{V}_{\text{eff}}(\mathbf{p}, \mathbf{r}), \quad (1)$$

where $m_{u/d}$ and m_s are the masses of u/d and s quarks, respectively, i.e., $m_u = m_d = 220$ MeV, $m_s = 419$ MeV. $\tilde{V}_{\text{eff}}(\mathbf{p}, \mathbf{r}) = \tilde{H}^{\text{conf}} + \tilde{H}^{\text{hyp}} + \tilde{H}^{\text{SO}}$ is the effective potential of the $q\bar{q}$ interaction which can be obtained from on-shell $q\bar{q}$ scattering amplitudes in the center-of-mass (CM) frame [2] and relativistic effect corrections. The quantities with tilde will be defined later. On the other hand $\tilde{V}_{\text{eff}}(\mathbf{p}, \mathbf{r})$ also consists

of two main parts. The first one is a $\gamma^\mu \otimes \gamma_\mu$ short-distance interaction of one-gluon exchange and the second part is a $1 \otimes 1$ long-distance color confining linear interaction, which is suggested by the lattice QCD [35–39].

In the nonrelativistic limit, $V_{\text{eff}}(\mathbf{p}, \mathbf{r})$ without tilde is transformed into the familiar nonrelativistic potential $V_{\text{eff}}(r)$ [2,40]

$$V_{\text{eff}}(r) = H^{\text{conf}} + H^{\text{hyp}} + H^{\text{so}} \quad (2)$$

with

$$H^{\text{conf}} = \left[-\frac{3}{4}(c + br) + \frac{\alpha_s(r)}{r} \right] (\mathbf{F}_1 \cdot \mathbf{F}_2)$$
$$= S(r) + G(r), \quad (3)$$

$$H^{\text{hyp}} = -\frac{\alpha_s(r)}{m_{u/d} m_s} \left[\frac{8\pi}{3} \mathbf{S}_1 \cdot \mathbf{S}_2 \delta^3(\mathbf{r}) + \frac{1}{r^3} \left(\frac{3\mathbf{S}_1 \cdot \mathbf{r} \mathbf{S}_2 \cdot \mathbf{r}}{r^2} \right. \right.$$
$$\left. \left. - \mathbf{S}_1 \cdot \mathbf{S}_2 \right) \right] (\mathbf{F}_1 \cdot \mathbf{F}_2), \quad (4)$$

$$H^{\text{so}} = H^{\text{so(cm)}} + H^{\text{so(tp)}}, \quad (5)$$

where H^{conf} is the spin-independent potential which contains a linear confining potential $S(r) = br + c$ and the one-gluon exchange potential $G(r) = -4\alpha_s(r)/3r$, H^{hyp} and H^{SO} are the color-hyperfine interaction and the spin–orbit interaction, respectively. It can be noted that $\mathbf{F}_1(\mathbf{F}_2) = \lambda_1(-\lambda_2^*)/2$, where λ_i is the Gell-Mann matrix. For the meson, $(\mathbf{F}_1 \cdot \mathbf{F}_2) = -4/3$. Additionally, the subscripts 1 and 2 denote quark and antiquark, respectively.

In Eqs. (3) and (4), the running coupling constant $\alpha_s(r)$ has the following form:

$$\alpha_s(r) = \sum_k \frac{2\alpha_k}{\sqrt{\pi}} \int_0^{\gamma_k r} e^{-x^2} \mathrm{d}x, \quad (6)$$

where k is from 1 to 3 and corresponding α_k and γ_k are constant, $\alpha_{1,2,3} = 0.25, 0.15, 0.2$ and $\gamma_{1,2,3} = \frac{1}{2}, \frac{\sqrt{10}}{2}, \frac{\sqrt{1000}}{2}$ [2]. For the color-hyperfine interaction H^{hyp}, the first term stands for contact interaction and second term is a typical form of tensor interaction, here $\mathbf{S}_1(\mathbf{S}_2)$ denotes the spin of the quark (antiquark).

In Eq. (5), the spin–orbit interaction can be divided into two types in which $H^{\text{so(cm)}}$ is the color-magnetic term and $H^{\text{so(tp)}}$ is the Thomas-precession term. Their expression can be written as

$$H^{\text{so(cm)}} = -\frac{\alpha_s(r)}{r^3} \left(\frac{1}{m_{u/d}} + \frac{1}{m_s} \right)$$
$$\times \left(\frac{\mathbf{S}_1}{m_{u/d}} + \frac{\mathbf{S}_2}{m_s} \right) \cdot \mathbf{L}(\mathbf{F}_1 \cdot \mathbf{F}_2), \quad (7)$$

$$H^{\text{so(tp)}} = -\frac{1}{2r} \frac{\partial H^{\text{conf}}}{\partial r} \left(\frac{\mathbf{S}_1}{m_{u/d}^2} + \frac{\mathbf{S}_2}{m_s^2} \right) \cdot \mathbf{L}, \quad (8)$$

---

[1] When studying the mass spectrum of the mesons, there are approaches like the Dyson–Schwinger and Bethe–Salpeter equations, which are directly related to QCD. However, such theory-based or theory-linked approaches still have some limitations in describing higher excitations of the mesons. Instead of theoretical approaches, one may apply phenomenological models to deal with such subjects. Here, the modified GI model is adopted to calculate the mass spectrum of pseudoscalar mesons.

where $\mathbf{L}$ is the orbital momentum between quark and antiquark.

Noting that the above interaction potentials are obtained in the nonrelativistic limit, and they can optimized by introducing the phenomenological relativistic effects. In the GI model, the relativistic effects are imposed into the model mainly by two ways. Firstly, a smearing function $\rho(\mathbf{r} - \mathbf{r}')$ is introduced to incorporate the effects of an internal motion inside a meson and nonlocality of interactions between quark and antiquark. A smearing transformation is given by

$$\tilde{f}(r) = \int d^3 r' \rho(\mathbf{r} - \mathbf{r}') f(r'), \tag{9}$$

with

$$\rho(\mathbf{r} - \mathbf{r}') = \frac{\sigma^3}{\pi^{3/2}} e^{-\sigma^2 (\mathbf{r} - \mathbf{r}')^2}, \tag{10}$$

$$\sigma = \sqrt{s^2 \left(\frac{2 m_{u/d} m_s}{m_{u/d} + m_s}\right)^2 + \sigma_0^2 \left(\frac{1}{2}\left(\frac{4 m_{u/d} m_s}{(m_{u/d} + m_s)^2}\right)^4 + \frac{1}{2}\right)}, \tag{11}$$

where $\sigma_0 = 1.80$ GeV and $s = 1.55$, are the universal parameters in the GI model, $f(r)$ is a arbitrary function and notation tilde stands for that the expression has been performed smearing transformation. By the smearing transformation, the one-gluon exchange potential $G(r) = -4\alpha_s(r)/(3r)$ and linear confined potential $S(r) = br + c$ are changed; thus

$$\tilde{G}(r) = -\sum_k \frac{8\alpha_k}{3\sqrt{\pi} r} \int_0^{\tau_k r} e^{-x^2} dx, \tag{12}$$

$$\tilde{S}(r) = br \left[\frac{e^{-\sigma^2 r^2}}{\sqrt{\pi} \sigma r} + \left(1 + \frac{1}{2\sigma^2 r^2}\right) \frac{2}{\sqrt{\pi}} \int_0^{\sigma r} e^{-x^2} dx \right] + c, \tag{13}$$

where

$$\tau_k = \frac{1}{\sqrt{\frac{1}{\sigma^2} + \frac{1}{\gamma_k^2}}}. \tag{14}$$

Secondly, a general expression of the potential should be dependent on the CM momentum of the interacting quarks. So the momentum-dependent effect is achieved by introducing momentum-dependent factors which will go to unity in the nonrelativistic limit. In a semiquantitative relativistic treatment, the smeared one-gluon exchange potential term $\tilde{G}(r)$ and the smeared hyperfine interactions (or spin–orbit interaction) $\tilde{V}^i$ should be modified with the following momentum-dependent factors:

$$G'(r) = \left(1 + \frac{p^2}{E_1 E_2}\right)^{1/2} \tilde{G}(r) \left(1 + \frac{p^2}{E_1 E_2}\right)^{1/2}, \tag{15}$$

$$\tilde{G}_{ij}^{so(v)} = \left(\frac{m_i m_j}{E_i E_j}\right)^{1/2 + \epsilon_{so(v)}} \tilde{G}(r) \left(\frac{m_i m_j}{E_i E_j}\right)^{1/2 + \epsilon_{so(v)}}, \tag{16}$$

$$\tilde{G}_{12}^c = \left(\frac{m_1 m_2}{E_1 E_2}\right)^{1/2 + \epsilon_c} \tilde{G}(r) \left(\frac{m_1 m_2}{E_1 E_2}\right)^{1/2 + \epsilon_c}, \tag{17}$$

$$\tilde{G}_{12}^t = \left(\frac{m_1 m_2}{E_1 E_2}\right)^{1/2 + \epsilon_t} \tilde{G}(r) \left(\frac{m_1 m_2}{E_1 E_2}\right)^{1/2 + \epsilon_t}, \tag{18}$$

$$\tilde{S}_{11}^{so(s)} = \left(\frac{m_1^2}{E_1^2}\right)^{1/2 + \epsilon_{so(s)}} \tilde{S}(r) \left(\frac{m_1^2}{E_1^2}\right)^{1/2 + \epsilon_{so(s)}}, \tag{19}$$

$$\tilde{S}_{22}^{so(s)} = \left(\frac{m_2^2}{E_2^2}\right)^{1/2 + \epsilon_{so(s)}} \tilde{S}(r) \left(\frac{m_2^2}{E_2^2}\right)^{1/2 + \epsilon_{so(s)}}, \tag{20}$$

where $E_1 = \sqrt{m_{u/d}^2 + p^2}$ and $E_2 = \sqrt{m_s^2 + p^2}$ are the energies of the quark and antiquark in the meson, and $m_1 = m_{u/d}$, $m_2 = m_s$, ϵ_i is parameter for a different type of hyperfine and spin–orbit interactions, which include the contact, tensor, vector spin–orbit and scalar spin–orbit potentials. Here, vector spin–orbit and scalar spin–orbit potentials correspond to Eq. (5) related to one-gluon exchange and confinement term, respectively. So the total Hamiltonian can be written as

$$\hat{H} = \left(p^2 + m_{u/d}^2\right)^{1/2} + \left(p^2 + m_s^2\right)^{1/2} + \tilde{H}^{conf} + \tilde{H}^{hyp} + \tilde{H}^{so} \tag{21}$$

with

$$\tilde{H}_{12}^{conf} = G'(r) + \tilde{S}(r), \tag{22}$$

$$\tilde{H}^{so} = \tilde{H}^{so(v)} + \tilde{H}^{so(s)}, \tag{23}$$

where

$$\tilde{H}^{so(v)} = \frac{\mathbf{S}_1 \cdot \mathbf{L}}{2m_{u/d}^2 r} \frac{\partial \tilde{G}_{11}^{so(v)}}{\partial r} + \frac{\mathbf{S}_2 \cdot \mathbf{L}}{2m_s^2 r} \frac{\partial \tilde{G}_{22}^{so(v)}}{\partial r} + \frac{(\mathbf{S}_1 + \mathbf{S}_2) \cdot \mathbf{L}}{m_{u/d} m_s} \frac{1}{r} \frac{\partial \tilde{G}_{12}^{so(v)}}{\partial r}, \tag{24}$$

$$\tilde{H}^{so(s)} = -\frac{\mathbf{S}_1 \cdot \mathbf{L}}{2m_{u/d}^2 r} \frac{\partial \tilde{S}_{11}^{so(s)}}{\partial r} - \frac{\mathbf{S}_2 \cdot \mathbf{L}}{2m_s^2 r} \frac{\partial \tilde{S}_{22}^{so(s)}}{\partial r}, \tag{25}$$

$$\tilde{H}_{12}^{hyp} = \tilde{H}_{12}^{tensor} + \tilde{H}_{12}^c, \tag{26}$$

where

$$\tilde{H}_{12}^{tensor} = -\left(\frac{\mathbf{S}_1 \cdot \mathbf{r} \mathbf{S}_2 \cdot \mathbf{r}/r^2 - \frac{1}{3}\mathbf{S}_1 \cdot \mathbf{S}_2}{m_{u/d} m_s}\right) \times \left(\frac{\partial^2}{\partial r^2} - \frac{1}{r} \frac{\partial}{\partial r}\right) \tilde{G}_{12}^t,$$

$$\tilde{H}_{12}^c = \frac{2\mathbf{S}_1 \cdot \mathbf{S}_2}{3 m_{u/d} m_s} \nabla^2 \tilde{G}_{12}^c.$$

For solving the Schrödinger equation, $\hat{H}\Psi = E\Psi$, with $\hat{H}$ shown in Eq. (21), the simple harmonic oscillators (SHO)

wave function will be employed. In the configuration space, the SHO wave function has the form

$$\Psi_{nLM_L}(\mathbf{r}) = R_{nL}(r, \beta)Y_{LM_L}(\Omega_r),$$
$$\Psi_{nLM_L}(\mathbf{p}) = R_{nL}(p, \beta)Y_{LM_L}(\Omega_p), \tag{27}$$

with

$$R_{nL}(r, \beta) = \beta^{3/2}\sqrt{\frac{2n!}{\Gamma(n + L + 3/2)}}(\beta r)^L e^{\frac{-r^2\beta^2}{2}}$$
$$\times L_n^{L+1/2}(\beta^2 r^2),$$
$$R_{nL}(p, \beta) = \frac{(-1)^n(-i)^L}{\beta^{3/2}}e^{-\frac{p^2}{2\beta^2}}$$
$$\times \sqrt{\frac{2n!}{\Gamma(n + L + 3/2)}}\left(\frac{p}{\beta}\right)^L L_n^{L+1/2}\left(\frac{p^2}{\beta^2}\right), \tag{28}$$

where $Y_{LM_L}(\Omega)$ is a spherical harmonic function with orbital angular momentum quantum number L, and $L_{n-1}^{L+1/2}(x)$ is an associated Laguerre polynomial, and β is a parameter of oscillator radial wave function. A series of SHO wave functions with different radial quantum numbers n can be regarded as a complete basis to expand the exact radial wave function of the meson state, in this case, the meson mass spectrum can be obtained by diagonalizing the Hamiltonian matrix of Eq. (21) by the above SHO basis. The total wave function of the meson is composed of color, flavor, spin, space wave function, and the spin wave functions χ are

$$\chi_{00} = \frac{1}{\sqrt{2}}(\uparrow\downarrow - \downarrow\uparrow),$$
$$\chi_{11} = \uparrow\uparrow,$$
$$\chi_{10} = \frac{1}{\sqrt{2}}(\uparrow\downarrow + \downarrow\uparrow),$$
$$\chi_{1-1} = \downarrow\downarrow. \tag{29}$$

The space-spin wave function $R_{nL}(r, \beta)\phi_{LSJM}$ with total angular quantum number J can be constructed by coupling $L \otimes S$ and has the form

$$\phi_{LSJM} = \sum_{M_L M_S} C(LM_L SM_S; JM)Y_{LM_L}(\Omega_r)\chi_{SM_S}, \tag{30}$$

where $C(LM_L SM_S; JM)$ is the Clebsch–Gordan coefficient. For the matrix element $\langle\alpha|\hat{V}(r, \hat{p})|\beta\rangle$ where $|\alpha\rangle$ and $|\beta\rangle$ are arbitrary SHO basis with quantum number $\{n, J, L, S\}$ and $\{n', J', L', S'\}$. It is noted that the color and flavor wave function of the meson have no contributions for the matrix element of Hamiltonian, and we have the general expression

$$\langle\alpha|\hat{V}(r, \hat{p})|\beta\rangle = \langle\alpha|f(p)g(r)|\beta\rangle$$
$$= \sum_n \langle\alpha|f(p)|n\rangle\langle n|g(r)|\beta\rangle. \tag{31}$$

After calculating each matrix element, the mass and wave function of meson could be obtained and they also are available for the following strong decay process.

Although the GI model has achieved great success in describing the meson spectrum, there still exists a discrepancy between the predictions given by the GI model and recent experimental observations. The previous work [5] presented a modified GI model with a screening potential whose predictions can be well consistent with the experimental data for the charm-strange mesons. For higher excitation states, the authors of Ref. [5] believe that a screening effect plays a very important role which could be introduced by the transformation $br + c \rightarrow \frac{b(1-e^{-\mu r})}{\mu} + c$, where μ is a screening parameter whose particular value is need to be fixed by the comparisons between theory and experiment. For a modified confinement potential one also needs to make a similar relativistic correction to the one mentioned in the GI model. Then we further write $V^{\text{scr}}(r)$ in the way given in Eq. (13),

$$\tilde{V}^{\text{scr}}(r) = \int d^3r' \rho(\mathbf{r} - \mathbf{r}')\frac{b(1 - e^{-\mu r'})}{\mu}. \tag{32}$$

By inserting the form of $\rho(\mathbf{r} - \mathbf{r}')$ in Eq. (11) into the above expression and finishing this integration, the concrete expression for $\tilde{V}^{\text{scr}}(r)$ is given by

$$\tilde{V}^{\text{scr}}(r) = \frac{b}{\mu r}\left[r + e^{\frac{\mu^2}{4\sigma^2}+\mu r}\frac{\mu + 2r\sigma^2}{2\sigma^2}\right.$$
$$\times\left(\frac{1}{\sqrt{\pi}}\int_0^{\frac{\mu+2r\sigma^2}{2\sigma}}e^{-x^2}dx - \frac{1}{2}\right)$$
$$-e^{\frac{\mu^2}{4\sigma^2}-\mu r}\frac{\mu - 2r\sigma^2}{2\sigma^2}$$
$$\left.\times\left(\frac{1}{\sqrt{\pi}}\int_0^{\frac{\mu-2r\sigma^2}{2\sigma}}e^{-x^2}dx - \frac{1}{2}\right)\right]. \tag{33}$$

It is worth mentioning that after the confinement potential is replaced with a screening potential, other treatments are similar to the original GI model including the calculation of matrix elements of the Hamiltonian.

2.2 The QPC model

The QPC model was first proposed by Micu [7] and further developed by the Orsay group [8,41–44]. This model was widely applied to the OZI-allowed two-body strong decay of hadrons in Refs. [9,10,13,15,17,19–24,27–30,32,33,45–49].

For a decay process $A \rightarrow B + C$, we can write

$$\langle BC|\mathcal{T}|A\rangle = \delta^3(\mathbf{P}_B + \mathbf{P}_C)\mathcal{M}^{M_{J_A}M_{J_B}M_{J_C}}, \quad (34)$$

where $\mathbf{P}_{B(C)}$ is a three-momentum of a meson $B(C)$ in the rest frame of a meson A. A superscript M_{J_i} ($i = A, B, C$) denotes an orbital magnetic momentum. The transition operator $\mathcal{T}$ is introduced to describe a quark–antiquark pair creation from vacuum, which has the quantum number $J^{PC} = 0^{++}$, i.e., $\mathcal{T}$ can be expressed as

$$\mathcal{T} = -3\gamma \sum_m \langle 1m; 1 - m|00\rangle \int d\mathbf{p}_3 d\mathbf{p}_4 \delta^3(\mathbf{p}_3 + \mathbf{p}_4)$$
$$\times \mathcal{Y}_{1m}\left(\frac{\mathbf{p}_3 - \mathbf{p}_4}{2}\right)$$
$$\times \chi_{1,-m}^{34} \phi_0^{34} \left(\omega_0^{34}\right)_{ij} b_{3i}^\dagger(\mathbf{p}_3) d_{4j}^\dagger(\mathbf{p}_4), \quad (35)$$

which is constructed in a completely phenomenological way to reflect the creation of a quark–antiquark pair from vacuum, where the quark and antiquark are denoted by indices 3 and 4, respectively. A dimensionless parameter γ depicts the strength of the creation of $q\bar{q}$ from vacuum; the concrete values of the parameter R will be discussed below. We have $\mathcal{Y}_{\ell m}(\mathbf{p}) = |\mathbf{p}|^\ell Y_{\ell m}(\mathbf{p})$, the solid harmonics. χ, ϕ, and ω denote the spin, flavor, and color wave functions respectively, which can be treated separately. Indices i and j denote the color of a $q\bar{q}$ pair.

By the Jacob–Wick formula [50], the decay amplitude is expressed as

$$\mathcal{M}^{JL}(\mathbf{P}) = \frac{\sqrt{4\pi(2L+1)}}{2J_A+1} \sum_{M_{J_B}M_{J_C}} \langle L0; JM_{J_A}|J_AM_{J_A}\rangle$$
$$\times \langle J_BM_{J_B}; J_CM_{J_C}|J_AM_{J_A}\rangle \mathcal{M}^{M_{J_A}M_{J_B}M_{J_C}}, \quad (36)$$

and the general decay width reads

$$\Gamma = \frac{\pi}{4}\frac{|\mathbf{P}|}{m_A^2}\sum_{J,L}|\mathcal{M}^{JL}(\mathbf{P})|^2, \quad (37)$$

where m_A is the mass of an initial state A. In our calculation, we need the spatial wave functions of the discussed kaons and iso-scalar and iso-vector light mesons. These can be numerically obtained by the modified GI model.

3 Mass spectrum analysis

Although the GI model has succeeded in describing the ground states of the kaon family, it does not well describe the excited states. Since unquenched effects are important for a heavy–light system, it is better to adopt the modified GI model (MGI) [5,6] which uses a screening potential with a new parameter μ. The parameter μ describes the inverse

Table 1 Parameters and their values in this work and GI models

Parameter	This work	GI [2]
b	0.2555	0.18
c	-0.3492	-0.253
μ	0.1	0
ϵ_{sov}	-0.01700	-0.035
ϵ_c	-0.1396	-0.168
ϵ_t	0.03600	0.025
ϵ_{sos}	0.06772	0.055

of the size of screening. To use the MGI model to calculate the kaon family spectra, it is better to determine the value of a new parameter μ considering two features: The first is when we use the same parameter set as in Ref. [2] and add a new parameter μ, the mass of the ground state of the kaon family will be lower than the experiments. The second one is that the value of μ may be not so small like as one in Refs. [5,6]. In fact, in bottomonium and charmonium states, Refs. [51,52] give a μ value of about 0.1 GeV, which is larger than the one in Refs. [5,6]. Since we do not know the real value of μ in the kaon family beforehand, we need to adjust the parameters by fitting with the experiments data. At first, the quark masses should be the same for all meson families. Secondly, we do not adjust the values of Λ and α_s for the same reason. Since σ_0 and s are universal parameters which are resolved by the $Q\bar{Q}$ system, we do not vary them in our fit. The confining term $br + c$ will be replaced by the screening potential, so their parameters should be fitted again. The relativistic effects should be adapted to a different system with the different quark masses. So we fix the following seven parameters listed in Table 1 by fitting 11 experimental data as listed in Table 2.

In Table 2, we select 11 experimental data of kaons listed in PDG and optimize these kaon masses to determine seven parameters in Table 1. This optimization has $\chi^2/n = 12.6$, which is smaller than 90.2 for the GI model as shown in Table 2. Another reason why we choose these kaons to fix the parameters in our model is that there does not exist a mixture between n^1L_L and n^3L_L states for these kaons. In order to obtain the optimum values of parameters and global and good fit of 11 data, we set "Error in fitting" in Table 2 so that the first two experimental data, corresponding to K and K^*, have artificial larger error values instead of the real errors in the brackets in the fourth column. The results listed in Table 2 show that the MGI model is better than the GI model since the value of χ^2/n of the MGI model is about 7 times smaller than that of the GI model and hence it is safely applied to describing the masses of the selected 11 kaons.

Although the MGI model is better than the GI model to depict 11 experimental data, we need to point out that there may exist a $\sim \mathcal{O}(100\ \text{MeV})$ deviation between experimen-

Table 2 The experimental data [1] fitted in our work. $\chi^2 = ((\text{Th} - \text{Exp})/\text{Error})^2$, where Th, Exp, and Error represent the theoretical, experimental results, and experimental error, respectively, and n is the number of the experimental data. We select some established kaon states in PDG [1] for our fitting. The unit of the mass is MeV

States	$n^{2S+1}L_J$	This work	GI [2]	Experiment [1]	Error in fitting
K	1^1S_0	497.7	461.5	497.6 ± 0.013	1.3
$K^*(892)$	1^3S_1	896	902.8	895.8 ± 0.19	1.9
$K_0^*(1430)$	1^3P_0	1257	1234	1425 ± 50	50
$K_2^*(1430)$	1^3P_2	1431	1428	1432.4 ± 1.3	1.3
$K^*(1680)$	1^3D_1	1766	1776	1717 ± 27	27
$K_3^*(1780)$	1^3D_3	1781	1794	1776 ± 7	7
$K_4^*(2045)$	1^3F_4	2058	2108	2045 ± 9	9
$K_5^*(2380)$	1^3G_5	2286	2388	$2382 \pm 14 \pm 19$	24
$K(1460)$	2^1S_0	1457	1454	1460	20
$K^*(1410)$	2^3S_1	1548	1579	1414 ± 15	15
$K_0^*(1950)$	2^3P_0	1829	1890	$1945 \pm 10 \pm 20$	22
χ^2/n		12.6	90.2		

tal and fitting results for several kaons, which is shown in Table 2. Such a difference of experimental and theoretical results may be due to the precision of the experiment. For example, there is only one experiment [1] for $K_5^*(2380)$ and $K_0^*(1950)$. The confirmation of $K_5^*(2380)$ and $K_0^*(1950)$ is still absent. Thus, further experimental measurement of the resonance parameters of these kaons will be helpful to clarify this difference of experimental and theoretical results.

By using the parameters shown in Table 1 as input, we further calculate the masses of other kaons, which are collected in Table 3, where we do not consider the mixing of states with n^1L_L and n^3L_L. Usually, there exists a mixture of the n^1L_L and n^3L_L states, i.e. [53]

$$\begin{pmatrix} |nL\rangle \\ |nL'\rangle \end{pmatrix} \approx \begin{pmatrix} \cos\theta_{nL} & \sin\theta_{nL} \\ -\sin\theta_{nL} & \cos\theta_{nL} \end{pmatrix} \begin{pmatrix} |n^1L_L\rangle \\ |n^3L_L\rangle \end{pmatrix}, \tag{38}$$

where $|nL\rangle$ and $|nL'\rangle$ are two mixing physical states and θ_{nL} is the corresponding mixing angle. Introducing such mixing states, we find two mass relations $m(nL) < m(n^1L_L)$ and $m(nL') > m(n^3L_L)$, which can be applied to identify these observed kaons with the same J^P quantum number. Thus, we need to combine the mass relations and mass spectrum of the kaons listed in Table 3 with the experimental data to further shed light on the properties of other observed kaons. We conclude that

1. Both $K_1(1270)$ with $M = (1272 \pm 7)$ MeV [1] and $K_1(1400)$ with mass $M = (1403 \pm 7)$ MeV [1] have $J^P = 1^+$ quantum numbers. $K_1(1270)$ and $K_1(1400)$ are the mixture of 1^1P_1 and 1^3P_1 states, i.e., $K_1(1270)$ and $K_1(1400)$ correspond to $1P$ and $1P'$ states, respectively.
2. $K_2(1770)$ has $J^P = 2^-$ and $M = (1773 \pm 8)$ MeV [1], while $K_2(1820)$ has $J^P = 2^-$ and $M = (1816 \pm 13)$ MeV [1]. $K_2(1770)$ and $K_2(1820)$, which correspond to

the $1D$ and $1D'$ states, respectively, are the mixture of the 1^1D_2 and 1^3D_2 states.

3. $K_1(1650)$ has $J^P = 1^+$ and $M = (1650 \pm 50)$ MeV [1]. Since the mass of $K_1(1650)$ is smaller than that of the 2^1P_1 state obtained in Table 3, thus we suggest that $K_1(1650)$ can be assigned as a $2P$ state. There must exist a partner, the $2P'$ state, which is still missing in experiments.
4. We suggest that $K(1830)$ is a 3^1S_0 state. Later, we will test this assignment by studying its decay behavior.
5. $K_2^*(1980)$ with $J^P = 2^+$ and $M = (2020 \pm 20)$ MeV [54] is either a 2^3P_2 state or a 1^3F_2 state.
6. $K_2(2250)$ with $J^P = 2^-$ and $M = (2247 \pm 17)$ MeV [1] is the candidate of $2D'$, which is the mixture of the 2^1D_2 and 2^3D_2 states.
7. $K_3(2320)$ has $J^P = 3^+$ and $M = (2324 \pm 24)$ MeV [1]. The possible assignment of $K_3(2320)$ is the $2F$ state, which is the mixture of states $K(2^1F_3)$ and $K(2^3F_3)$. As the partner of $K_3(2320)$, $K(2F')$ is till absent in experiments. In addition, we should mention that $1F$ and $1F'$ in the kaon family are still missing.
8. $K_4(2500)$ with $J^P = 4^-$ and $M = (2490 \pm 20)$ MeV [1] can be a $2G$ state, while its partner $K(2G')$ and two kaons $K(1G)$ and $K(1G')$ are still missing in experiments.

Surely, the above conclusions of possible quantum states are only from the point of mass spectra view. If we want to clearly study particle properties further, we also need to investigate the decay behaviors, especially strong decays, and a detailed study will be given in the next section.

4 OZI-allowed two-body strong decays

In the previous section, calculating the spectra of the kaon family, we obtain kaon wave functions, too, at the same time,

Table 3 The masses of other kaons obtained by the MGI model and comparison with those from other potential models. The unit of the mass is MeV

$n^{2S+1}L_J$	This work	GI [2]	Ref. [4]	Ref. [3]	$n^{2S+1}L_J$	This work
1^1P_1	1364	1352	–	–	3^1D_2	2380
1^3P_1	1377	1366	–	–	3^3D_1	2385
1^1D_2	1778	1791	1709	–	3^3D_2	2388
1^3D_2	1789	1804	1824	–	3^3D_3	2382
1^1F_3	2075	2131	2009	2050	3^1F_3	2550
1^3F_2	2093	2151	1964	2050	3^3F_2	2560
1^3F_3	2084	2143	2080	2050	3^3F_3	2546
1^1G_4	2309	2422	2255	–	3^3F_4	2533
1^3G_3	2336	2458	2207	–	3^1G_4	2673
1^3G_4	2317	2433	2285	–	3^3G_3	2687
2^1P_1	1840	1897	1757	1850	3^3G_4	2677
2^3P_1	1861	1928	1893	1850	3^3G_5	2662
2^3P_2	1870	1938	1896	1850	4^1S_0	2248
2^1D_2	2121	2238	2066	–	4^3S_1	2287
2^3D_1	2127	2251	2063	–	4^1P_1	2422
2^3D_2	2131	2254	2163	–	4^3P_0	2424
2^3D_3	2121	2237	2182	–	4^3P_1	2434
2^1F_3	2340	2524	2348	–	4^3P_2	2438
2^3F_2	2356	2551	–	–	4^1D_2	2570
2^3F_3	2347	2536	–	–	4^3D_1	2573
2^3F_4	2328	2504	2436	–	4^3D_2	2575
2^1G_4	2520	2779	2575	–	4^3D_3	2571
2^3G_3	2540	2814	–	–	4^1F_3	2688
2^3G_4	2526	2789	–	–	4^3F_2	2695
2^3G_5	2504	2749	–	–	4^3F_3	2691
3^1S_0	1924	2065	–	1860	4^3F_4	2683
3^3S_1	1983	2156	1950	–	4^1G_4	2782
3^1P_1	2177	2164	–	–	4^3G_3	2790
3^3P_0	2176	2160	–	–	4^3G_4	2785
3^3P_1	2192	2200	–	–	4^3G_5	2776
3^3P_2	2198	2206	–	–		

which can be used in the QPC model to study the strong decay of the kaon family. The parameter γ in the QPC model is determined by fitting with the experimental data [47]. Thus, there is no free parameter in the QPC model. We obtain $\gamma = 10.5$ as shown in Table 4.

In the following, we mainly focus on the OZI-allowed two-body strong decay behaviors of these discussed kaons, by which we not only test these possible assignments to the observed kaons, but also provide more abundant predictions of higher radial and orbital excitations in the kaon family.

4.1 S-wave kaons

Since $K(498)$ and $K^*(892)$ were established to be the 1^1S_0 and 1^3S_1 states in the kaon family, respectively, in this work

we do not discuss them, but we present the phenomenological analysis of the $2S$ and $3S$ states.

4.1.1 2S states

As the candidate of the 2^1S_0 state, $K(1460)$ was listed in PDG. If further checking the experimental data, we find that $K(1460)$ was only reported in Refs. [55,56]. However, in the past 30 years, further experiment as regards $K(1460)$ was missing, which is the reason why $K(1460)$ was removed from the summary table of the PDG.

In Table 5, we give the information on the partial and total decay widths of $K(1460)$ as an 2^1S_0 state, in which one can find $K(1460)$ mainly decays into $K^*\pi$, $K\rho$, and $K\omega$. Here, our results are larger than the experimental data for $K^*\pi$,

Table 4 The parameter γ fitting in the QPC model. The unit of the width is MeV

Channels	Experimental data	Numerical result
$K^* \to K\pi$	50.2 ± 5	33.5
$K_0^*(1430) \to K\pi$	267 ± 36	314
$K_2^*(1430) \to K\pi$	48.9 ± 1.7	51.5
$K_2^*(1430) \to K^*\pi$	24.8 ± 1.7	20.4
$K_2^*(1430) \to K\rho$	8.7 ± 0.8	6.13
$K_2^*(1430) \to K\omega$	2.9 ± 0.8	1.82
$K_3^*(1780) \to K\rho$	74 ± 10	20.1
$K_3^*(1780) \to K^*\pi$	45 ± 7	28.5
$K_3^*(1780) \to K\pi$	31.7 ± 3.7	38.1
$K_4^*(2045) \to K\pi$	19.6 ± 3.8	21.0
$K_4^*(2045) \to K\phi$	2.8 ± 1.4	3.80
	$\chi^2 = 6.8, \gamma = 10.5$	

Table 5 The strong decay widths of the $2S$ and $3S$ states. The unit of the width is MeV

States	Channels	This work	Experiment
$K(1460)\,[2^1S_0]$	$K^*\pi$	248	~ 109 [55]
	$K\rho$	161	~ 34 [55]
	$K\omega$	51.2	–
	$K^*\eta$	8.0	–
	Total	468	~ 260 [55]
$K^*(1410)\,[2^3S_1]$	$K^*\pi$	81.8	–
	$K\rho$	47.4	–
	$K\omega$	14.8	–
	$K\pi$	34.7	–
	$K\eta$	35.4	–
	Total	214	232 ± 21 [1]
	$\Gamma_{K\pi}/\Gamma_{\text{Total}}$	16.2%	$(6.6 \pm 1 \pm 0.8)\%$
$K(1830)\,[3^1S_0]$	$K^*(1410)\pi$	105	–
	$K^*\pi$	34.7	–
	$K_0^*(1430)\pi$	29.8	–
	$K\rho$	22.4	–
	$K_2^*(1430)\pi$	21.7	–
	$K^*\rho$	17.4	–
	$K\omega$	7.07	–
	$K^*\omega$	6.0	–
	$K^*\eta$	1.26	–
	$K\phi$	0.018	–
	Total	245	~ 250 [1]
3^3S_1	$K^*(1410)\pi$	62.3	–
	$K^*\pi$	44.2	–
	$K\rho$	36.8	–
	$K_2^*\pi$	29.4	–
	$K\pi$	23.3	–
	$K(1460)\pi$	20.8	–
	$K\eta(1295)$	18.5	–
	Ka_2	15.8	–
	$K\pi(1300)$	14	–
	$K\eta$	13.1	–
	$K\omega$	12	–
	$K_1(1650)\pi$	11.8	–
	Kb_1	11.6	–
	$\eta K_1(1400)$	7.93	–
	$K_1\eta$	7.93	–
	Ka_1	7.76	–
	Kf_2	7.65	–
	$K\omega(1420)$	7.62	–
	$Kf_1(1420)$	7.18	–
	$K^*\phi$	5.54	–
	$K\rho(1450)$	5.46	–
	Kh_1	4.22	–

$K\rho$, and the total width. If we are to establish $K(1460)$ as an 2^1S_0 state, we need to clarify these differences between our calculation and the experimental data. We expect an independent experiment to confirm the observation of $K(1460)$. Especially, we suggest precise measurement of the resonance parameters and partial decay widths of $K(1460)$.

In the PDG, $K^*(1410)$ is a possible candidate of the 2^3S_1 state. However, we must face the following puzzling facts: (1) the mass of $K^*(1410)$ is smaller than that of $K(1460)$. Usually, an 2^3S_1 state has mass higher than that of an 2^1S_0 state. In addition, we also notice the theoretical results of the mass of an 2^3S_1 state [2,4] and this work gives the mass of an 2^3S_1 state to be 1579, 1675, 1548, and 1580 MeV, respectively, all of which are larger than the experimental data, 1414 MeV, if $K^*(1410)$ is an 2^3S_1 state. Thus, we need to understand why there exists such a puzzling mass relation for $K^*(1410)$ and $K(1460)$. (2) If $K^*(1410)$ together with $\rho(1450)$, $\omega(1420)$, and $\phi(1680)$ forms an 2^3S_1 nonet, one can notice that the mass of $K^*(1410)$ as an 2^3S_1 state is a bit small, which was also indicated in Ref. [3].

In Table 5, the obtained partial and total decay widths of $K^*(1410)$ as an 2^3S_1 are given, where we also compare our result with the experimental data. The main decay modes of $K^*(1410)$ include the $K\pi$, $K^*\pi$, $K\rho$, and $K\eta$ channels. The obtained total decay width of $K^*(1410)$ is consistent with the experiment result. We also notice that the ratio $\Gamma_{K\pi}/\Gamma_{\text{Total}}$ obtained in this work is a little bit larger than the experimental value ($\Gamma_{K\pi}/\Gamma_{\text{Total}} = (6.6 \pm 1 \pm 0.8)\%$). The above result is gotten by assuming $K^*(1410)$ to be an 2^3S_1 pure state. In fact, $K^*(1410)$ could be a mixture of the 2^3S_1 and 1^3D_1 states. Thus, in the following, we further discuss such an S–D mixing effect on the ratio $\Gamma_{K\pi}/\Gamma_{\text{Total}}$ of $K^*(1410)$. $K^*(1410)$ and $K^*(1680)$ as a mixture of the 2^3S_1 and 1^3D_1 states can be expressed as

Table 5 continued

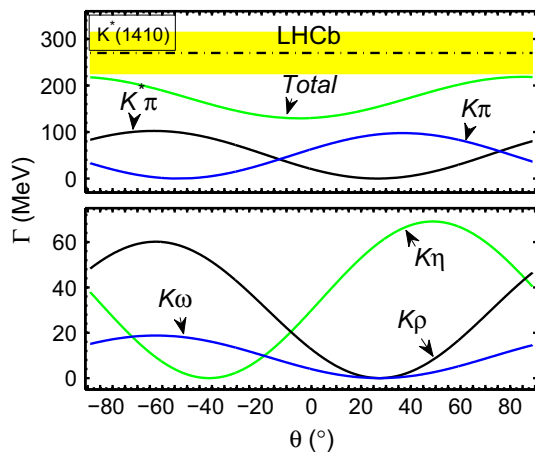| States	Channels	This work	Experiment
	$K_1(1400)\pi$	3.82	–
	$K_1\pi$	3.82	–
	$K^*\rho$	3.38	–
	Kf_1	2.92	–
	$K\phi$	2	–
	Total	393	–

Fig. 1 The θ_{sd} dependence of the total and partial decay widths of $K^*(1410)$. Here, the dot-dashed line is the experimental value from LHCb [57]

$$\begin{pmatrix} |K^*(1410)\rangle \\ |K^*(1680)\rangle \end{pmatrix} = \begin{pmatrix} \cos\theta_{sd} & \sin\theta_{sd} \\ -\sin\theta_{sd} & \cos\theta_{sd} \end{pmatrix} \begin{pmatrix} |1^3D_1\rangle \\ |2^3S_1\rangle \end{pmatrix}, \quad (39)$$

where θ_{sd} denotes the mixing angle. In this scenario, we present the decay behavior of $K^*(1410)$ dependent on θ_{sd} as shown in Fig. 1. The result shows that the experimental total width [57] of $K^*(1410)$ can be described when θ_{sd} is taken as $\sim 90°$ or $\sim -90°$, which supports $K^*(1410)$ as a pure 2^3S_1 state. We need to emphasize that the branching ratio $\Gamma_{K\pi}/\Gamma_{\text{Total}}$ becomes larger when $|\theta_{sd}|$ becomes smaller. Thus, the S–D mixing effect on the $K^*(1410)$ state is not obvious on describing the experimental data. Of course, we must admit that there still exists a small difference between theoretical and experimental results for the ratio $\Gamma_{K\pi}/\Gamma_{\text{Total}}$.

Finally, we give a conclusion for $K^*(1410)$. The mass of $K^*(1410)$ as a 2^3S_1 state is relatively small, and there exists some disagreement in the branching ratios with experiments. Obviously, confirmation of this state assignment needs more experimental information and theoretical study.

4.1.2 3S states

Although $K(1830)$ is not listed in the summary table of the PDG, we still select $K(1830)$ as a possible candidate of the 3^1S_0 state and study its decay behavior.

In Table 5, the partial and total decay widths of $K(1830)$ as a 3^1S_0 state are shown. Our results show that the largest decay width of $K(1830)$ is given by the channel $K^*(1410)\pi$ instead of $K^*\rho$ given by Ref. [3]. The other main decay channels contain $K^*\pi$, $K_0^*(1430)\pi$, $K\rho$, $K_2^*(1430)\pi$, and $K^*\rho$. The total width of the theory agrees with the experimental data. Our prediction of the decay information on this state will be helpful for future experimental study, since there exist only two experimental studies on $K(1830)$ until now.

At present, the 3^3S_1 state in the kaon family is still absent. Thus, in this work we predict its decay property, where we take the predicted mass of the 3^3S_1 state by the MGI model as the input. The results shown in Table 5 indicate that its important decay modes are $\pi K^*(1410)$, $K^*\pi$, $K\rho$, and $K_2^*\pi$, $K\pi$, $\pi K(1460)$, $K\eta(1295)$. Additionally, Ka_2 also has a sizable contribution to the total width. This predicted decay information is useful to the future experimental search for this missing state.

4.2 P-wave kaons

4.2.1 1P states

In Table 6, we show the allowed decay channels of $K_0^*(1430)$, and the corresponding partial and total decay widths. Here, its dominant decay channel of $K_0^*(1430)$ is $K\pi$, which has decay width 314 MeV, which is comparable with the experimental data (267 ± 36) MeV listed in PDG [1]. Besides, the $K\eta$ decay channel also has a sizable contribution to the total decay width of $K_0^*(1430)$. In addition, the obtained total decay width is consistent with the experimental measurement just shown in Table 6. The above study indicates that the 1^3P_0 assignment to $K_0^*(1430)$ is suitable.

The $K_2^*(1430)$ together with $a_2(1320)$, $f_2(1270)$, and $f_2'(1525)$ may form a 1^3P_2 nonet. In Table 6, we give the partial decay widths of $K_2^*(1430)$. It dominantly decays into $K\pi$ and $K^*\pi$, while the $K\rho$, $K\omega$, and $K\eta$ modes also have sizable contributions in which $K\eta$ was already observed in experiment [1]. According to Table 6, we can find that our results are consistent with the experimental data. Thus, $K_2^*(1430)$ as a 1^3P_2 state in the kaon family can be supported by our study of its decays.

$K_1(1270)$ and $K_1(1400)$ as the $1P$ and $1P'$ states, respectively, satisfy

$$\begin{pmatrix} |K_1(1270)\rangle \\ |K_1(1400)\rangle \end{pmatrix} \approx \begin{pmatrix} \cos\theta_{1P} & \sin\theta_{1P} \\ -\sin\theta_{1P} & \cos\theta_{1P} \end{pmatrix} \begin{pmatrix} |1^1P_1\rangle \\ |1^3P_1\rangle \end{pmatrix}, \quad (40)$$

Table 6 The decay widths of three P-wave states. The unit of the width is MeV

States	Channels	This work	Experiment
$K_0^*(1430)\ [1^3P_0]$	$K\pi$	314	267 ± 36 [58]
	Kη	2.87	–
	Total	318	270 ± 80 [1]
$K_2^*(1430)\ [1^3P_2]$	$K\pi$	51.5	48.9 ± 1.7 [1,47]
	$K^*\pi$	20.4	24.8 ± 1.7 [1,47]
	$K\rho$	6.13	8.7 ± 0.8 [1,47]
	$K\omega$	1.82	2.9 ± 0.8 [1,47,59]
	$K\eta$	0.0665	$0.15^{+0.37}_{-0.1}$ [1]
	Total	80.1	98.5 ± 2.9 [1]
$K_0^*(1950)\ [2^3P_0]$	$K\pi$	105	–
	$K^*\rho$	254	–
	$K\pi(1300)$	190	–
	$K(1460)\pi$	121	–
	Ka_1	69.1	–
	Kb_1	64.9	–
	$K_1(1270)\pi$	183	–
	$K_1(1270)\eta$	6.58	–
	$K_1(1400)\pi$	5.98	–
	Total	1000	$201 \pm 34 \pm 79$ [58]
	$\Gamma_{K\pi}/\Gamma_{\text{Total}}$	10.5%	$(52 \pm 8 \pm 12)\%$ [58]

where θ_{1P} denotes the mixing angle, which leads us to discuss the θ_{1P} dependence of the partial and total decay widths of $K_1(1270)$ and $K_1(1400)$.

According to Fig. 2 which describes the dependence of the mixing angle, θ_{1P}, of the $K_1(1270)$ decay width, we find that θ_{1P} should be taken as either $22.5°$–$29°$ or $41.5°$–$48°$ by fitting the CNTR data of $\Gamma_{K^*\pi}$ [55], which is fortunately in the same range when fitted with the ratio $\Gamma(K^*\pi)_{D\text{-wave}}/\Gamma(K^*\pi)_{S\text{-wave}} = 1 \pm 0.7$ [55]. Here, the central value of this mixing angle is $\theta_{1P} \approx 25°$ or $45°$.

We further investigate the decays of $K_1(1400)$. CNTR [55] also gave $\Gamma_{K^*\pi}/\Gamma_{\text{Total}} = (94 \pm 6)\%$ [60] for $K_1(1400)$, by which we obtain $38° < \theta_{1P} < 68°$ with central value $\theta_{1P} = 45°$, where the details can be found in Fig. 3.[2] Hence, the above analysis shows that the mixing angle θ_{1P} favors $45°$, which agrees with the conclusion made in Refs. [3,47] but disagrees with Refs. [61–63], in which they obtained $\theta_{1P} = 34°$ and $\sim 60°$, respectively.

---

[2] CNTR [55] gave $\Gamma_{K^*\pi(D)}/\Gamma_{K^*\pi(S)} = 0.04 \pm 0.01$ as well, which gives the angle range $-7°$ to $0°$ or $70°$ to $78°$ if we fit with the ratio, which conflicts with the previous discussion.
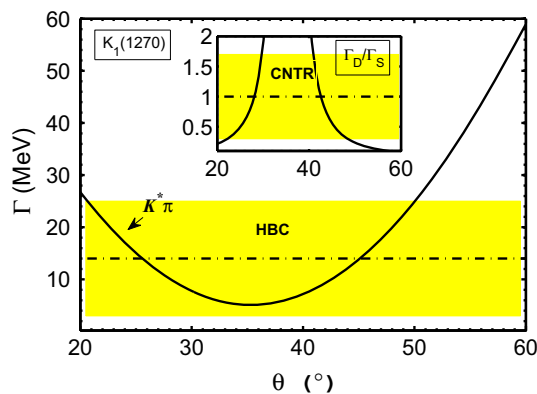
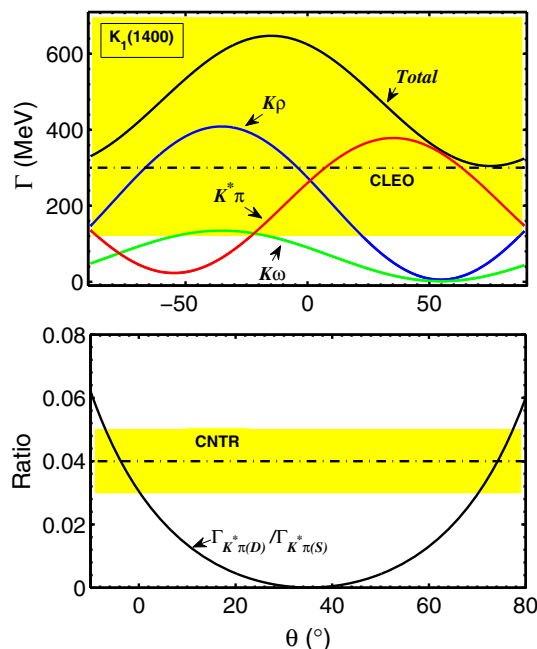**Fig. 2** θ_{1P} dependence of the $K_1(1270) \rightarrow K^*\pi$ decay width

Fig. 3 θ_{1P} dependence of the partial, the total decay widths and ratio $\Gamma_{K^*\pi(D)}/\Gamma_{K^*\pi(S)}$ of $K_1(1400)$

4.2.2 2P states

As shown in Table 3, Refs. [2–4] and this work give the mass of the 2^3P_0 state 1.890, 1.791, 1.850, and 1.829 GeV, respectively, which are all smaller than the experimental value 1945 MeV if $K_0^*(1950)$ is assumed to be a 2^3P_0 state. Under the assignment of the 2^3P_0 state to $K_0^*(1950)$, we study the strong decay behavior of $K_0^*(1950)$, which is presented in Table 6.

Our results show that the $K^*\rho$ mode is its dominant decay channel. Its total decay width can reach up to 1000 MeV which is 5 times larger than the experimental value 200 MeV. We also notice the result of the total decay width of a 2^3P_0 state given by Ref. [3], which is two times larger than the experimental value, where they use a smaller phase space

Table 7 The strong decay widths of $K_2^*(1980)$, where the values in brackets and without brackets in the third and fourth columns represent those for $K_2^*(1980)$ as the 1^3F_2 and 2^3P_2 states, respectively. The unit of the width is MeV

States	Channel	This work	Ref. [3]	Experiment
$K_2^*(1980)$	$K_1(1270)\pi$	36.5 (55.7)	6 (79)	–
	$K_2(1770)\pi$	0.473 (5.67)	− (61)	
	Kb_1	24.1 (36.7)	8 (50)	–
	Ka_1	11.8 (10.8)	3 (26)	–
	$K_1(1270)\eta$	6.31 (5.57)	1 (22)	–
	$K\pi$	0.788 (17.5)	44 (20)	–
	Kh_1	11.8 (9.00)	4 (18)	–
	$K\rho$	10.6 (18.3)	4 4 (13)	–
	$K^*\pi$	10.2 (16.2)	47 (13)	–
	$K\eta'$	3.50 (6.51)	15 (15)	–
	$K^*\eta$	24.6 (6.80)	26 (11)	–
	$K_2^*(1425)\pi$	61.3 (17.4)	15 (8)	–
	$K^*\rho$	42.1 (17.1)	78 (8)	–
	$Kf_1(1282)$	2.93 (2.67)	1 (7)	–
	Ka_2	28.4 (11.8)	3(7)	–
	$Kf_1(1426)$	0.454 (0.32)	− (6)	–
	$K\phi$	11.1 (3.31)	12 (6)	–
	$K\omega$	3.60 (6.09)	14 (4)	–
	$Kf_2(1270)$	12.1 (5.55)	3 (3)	–
	$K^*\omega$	22.0 (5.42)	27 (3)	–
	$K^*\phi$	41.0 (0.109)	− (1)	–
	$K_1(1400)\pi$	7.56 (7.32)	11 (0)	–
	$K^*(1410)\pi$	63.9 (2.03)	5 (0)	–
	$\pi K(1460)$	27.9 (4.31)	2 (0)	–
	$K\pi(1300)$	15.0 (5.57)	0 (0)	–
	Total	480 (278)	370 (283)	$373 \pm 33 \pm 60$ [64] (180 ± 70 [54])
	$\Gamma_{K\rho}/\Gamma_{K^*\pi}$	1.04 (1.14)	0.94 (1)	$1.49 \pm 0.24 \pm 0.09$ [58] (–)

(their mass of a 2^3P_0 state is 1850 MeV). We also obtain the branching ratio $\Gamma_{K\pi}/\Gamma_{\text{Total}} = 6.4\%$, which is close to 10.5% calculated by Ref. [3], but this is smaller than the experimental value 52%. Besides, we also confirm that $K_1(1270)\pi$ has sizable contribution to the width of $K_0^*(1950)$ [3]. It is obvious that there exists a difference between the present theoretical and experimental results. Until now, $K_0^*(1950)$ has not been established in experiment since this state was omitted from the summary table of PDG [1]. For clarifying it, we suggest further experimental study of $K_0^*(1950)$, where its resonance parameter and partial decay widths are crucial information.

Then we discuss the possibility of two different assignments to $K_2^*(1980)$ from two aspects, mass and decay information. In 1987, LASS reported a structure in the reaction $K^-p \rightarrow \bar{K}^0\pi^+\pi^-n$ [64], and the obtained resonance parameter are $M = (1973 \pm 8 \pm 25)$ MeV and $\Gamma = (373 \pm 33 \pm 60)$ MeV. This is the particle called $K_2^*(1980)$ listed by the PDG [1]. Barnes et al. [3] take the viewpoint that $K_2^*(1980)$ is a 1^3F_2 state, and they give a

total width of 300 MeV. However, our results show that the mass of a 1^3F_2 state is about 2093 MeV. Thus, the mass of $K_2^*(1980)$ is a bit small if $K_2^*(1980)$ is a 1^3F_2 state, which can be supported by another fact, i.e., as an iso-vector 1^3F_2 state, $a_2(2030)$ is well established in Ref. [32]. In the same 1^3F_2 nonet, the meson which contains one s quark is heavier than the mesons which only contain u/d quarks. Along this line, the mass of the 1^3F_2 state in the kaon family should be heavier than 2030 MeV.

Assuming the 1^3F_2 state assignment to $K_2^*(1980)$, we illustrate its decay behavior. The present work (see Table 7) shows that $K_1(1270)\pi$ is the dominant decay channel when we treat $K_2^*(1980)$ as a 1^3F_2 state, even though the channel is not observed in experiments. The $K_2(1770)\pi$, Kb_1, Ka_1, $K\pi$, $K\rho$, and $K^*\pi$ modes, among which $K\rho$ and $K^*\pi$ have been reported in the experiment [1], also have sizable contributions, where we take $\theta_{1D} = -39°$. Our prediction for the channels $K_1(1270)\pi$, $K_2(1770)\pi$, Kb_1, Ka_1, and $K\pi$ will be helpful for the experimental test of this assignment.
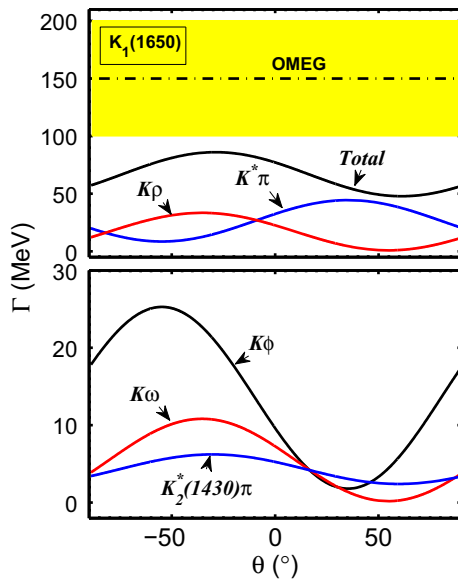
Fig. 4 θ_{2P} dependence of the decay widths of $K_1(1650)$ as a $2P$ state, where the dot-dashed line is the experimental value of OMEG [65]

Fig. 5 θ_{2P} dependence of the decay widths of $K_1(1650)$ as a $2P$ state with the measured center mass of 1793 MeV from LHCb [66], where the dot-dashed line is the experimental value of LHCb [66]

Besides the assignment of the 1^3F_2 state to $K_2^*(1980)$, there exists another possibility, $K_2^*(1980)$ as a 2^3P_2 state. The analysis of the mass spectra in Refs. [2–4] and this work shows that the mass of a 2^3P_2 state is 1938, 1896, 1850, and 1870 MeV, respectively. Thus, the experimental mass value of $K_2^*(1980)$ is a bit larger than a 2^3P_2 state. If $K_2^*(1980)$ is a 2^3P_2 state, its main decay modes are $K^*\rho$, $K\pi$, $K^*\pi$, $K\rho$, $K^*\eta$, $K\eta'$, and $K^*\omega$. Besides the $K\rho$ and $K^*\pi$ modes, one notices that Kf_2 has been observed in experiments, which has a sizable contribution in theory. Hence, $K_2^*(1980)$ as a 2^3P_2 state is also a possible assignment.

Just presented above, we discuss two assignments to $K_2^*(1980)$, where the decay behaviors of $K_2^*(1980)$ under two assignments are different. Thus, we should combine further experimental decay information of $K_2^*(1980)$ with our results to determine which possibility of its assignments we should take.

The $K_1(1650)$ and its partner $K_1(2P')$ satisfy

$$\begin{pmatrix} |K_1(1650)\rangle \\ |K_1(2030)\rangle \end{pmatrix} \approx \begin{pmatrix} \cos\theta_{2P} & \sin\theta_{2P} \\ -\sin\theta_{2P} & \cos\theta_{2P} \end{pmatrix} \begin{pmatrix} |2^1P_1\rangle \\ |2^3P_1\rangle \end{pmatrix}. \quad (41)$$

In Fig. 4, we show the partial and total decay widths of $K_1(1650)$ depending on the mixing angle θ_{2P} if the mass of $K_1(1650)$ is adored to be $M = 1650 \pm 50$ MeV [1]. Since the decays of $K_1(1650)$ into $K\pi\pi$ and $K\phi$ were observed in experiments [55,65–67], we can roughly conclude that θ_{2P} is probably less than zero as seen from Fig. 4, where $K\rho$, $K\phi$ and $K^*\pi$ have sizable contributions to the total decay width of $K_1(1650)$ in our calculation.

In experiment, $K_1(1650)$ is also not well established since this state is omitted from the summary table of the PDG [1].
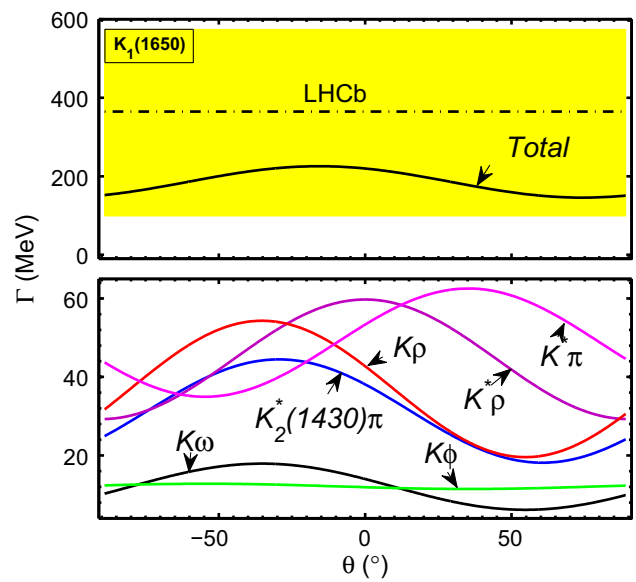
More experimental and theoretical efforts are necessary to establish $K_1(1650)$. We notice new experimental information of $K_1(1650)$ from LHCb [66], where the measured mass of $K_1(1650)$ is $(1793 \pm 59^{+153}_{-101})$ MeV, which is about 150 MeV larger than the experimental data given by Ref. [1]. Taking the LHCb mass result as an input, we investigate the strong decay behaviors of $K_1(1650)$ again, which are shown in Fig. 5. Here, $K^*\pi$, $K^*\rho$, $K\rho$ and $K_2^*(1430)\pi$ are dominant decay channels. However, we cannot give a further constraint on the mixing angle θ_{2P} by comparing an experimental width with our theoretical result due to a large experimental error of the LHCb experimental data.

In the following, we discuss the partner of $K_1(1650)$. Reference [68] gives the following equation for the mass relation between the pure states and physical state:

$$m^2_{K_1(2^3P_1)} = \cos(\theta_{2P})^2 m^2_{K_1(2P')} + \sin(\theta_{2P})^2 m^2_{K_1(2P)},$$
$$m^2_{K_1(2^1P_1)} = \sin(\theta_{2P})^2 m^2_{K_1(2P')} + \cos(\theta_{2P})^2 m^2_{K_1(2P)}. \quad (42)$$

Substituting $m_{K_1(2^1P_1)} = 1840$ MeV and $m_{K_1(2^3P_1)} = 1861$ MeV given in Table 3 into Eq. (42), we obtain the mass of the $K_1(1650)$ partner, $m_{K_1(2P')}$, about 2030 MeV and the $\theta_{2P} \approx \pm 43°$ if taking the mass of $K_1(1650)$ as $M = (1650 \pm 50)$ MeV [1]. Based on the above analysis of $K_1(1650)$, we suggest $\theta_{2P} \approx -43°$. If taking the LHCb mass measurement [66] of $K_1(1650)$ as an input, the mass of the $K_1(1650)$ partner is estimated to be 1906 MeV. In Ref. [66], the resonance parameters of the $K_1(1650)$ partner are given, i.e., $M = (1968 \pm 65^{+70}_{-172})$ MeV and $\Gamma = (396 \pm 170^{+174}_{-178})$ MeV. Considering the present status, we select the experimental mass (1968 MeV [66]) for the partner of $K_1(1650)$

Table 8 The main strong decay widths of the $K_1(2P')$ state which as the partner of $K_1(1650)$. Here, the mass of $K_1(2P')$ is taken as 1968 MeV [66]. $c = \cos\theta_{2P}$ and $s = \sin\theta_{2P}$. The unit of the width is MeV

Decay channel	Width
Total	$440\,c^2 + 70.2\,c\,s + 385\,s^2$
$K^*\rho$	$166\,c^2 + 111s^2$
$K_2^*\pi$	$71.5\,c^2 + 57\,c\,s + 111\,s^2$
$K\,a_2$	$59c^2 + 48.\,c\,s + 80.8\,s$
$K^*\pi$	$75.4\,c^2 + 8.84\,c\,s + 72.3\,s^2$
$K\rho$	$63.1\,c^2 + 2.81\,c\,s + 64.1\,s^2$
$K^*\omega$	$53.8\,c^2 + 36s^2$
Kf_2	$22.4\,c^2 + 10.5\,c\,s + 20.8\,s^2$

when discussing the decay behavior of the $K_1(2P')$ state just shown in Table 8. Here, the calculated width of $K_1(2P')$ is about (440–570) MeV, which is comparable to the experimental data [66]. Its main decay modes are $K^*\rho$, $K_2^*\pi$, Ka_2, $K^*\pi$, $K\rho$, $K^*\omega$, and Kf_2.

4.3 D-wave kaons

4.3.1 1D states

$K^*(1680)$ together with $\rho(1700)$ and $\omega(1650)$ forms a 1^3D_1 nonet. Barnes et al. [3] predicted that this state should have a mass of 1850 MeV, but we obtain 1.766 GeV, which is closer to the experimental value 1.717 GeV. The mass spectrum analysis supports $K^*(1680)$ as a 1^3D_1 state.

As shown in Table 9, $K^*(1680)$ as a pure 1^3D_1 state mainly decays into final states $K_1(1270)\pi$, Kh_1, $K\pi$, and $K\eta$, while the $K^*\pi$ and $K\rho$ modes also have sizable contributions. We notice that the obtained ratios of partial decay widths of $K\pi$, $K^*\pi$, and $K\rho$ in this work are comparable with experimental data given in PDG. Since the branching ratios of the $K\pi$, $K^*\pi$, and $K\rho$ decay channels given by PDG are 38.7, 29.9, and 31.4%, we conclude that the remaining $K_1(1270)\pi$ decay channel has a very small width. However, our calculation shows that $K_1(1270)\pi$ is a main contribution to the total width which is consistent with the conclusion from the former analysis in [3] but contradicts the present experimental data. Here we and the authors of Ref. [3] adopted the mixing angle $\theta_{1P} = 45°$ [4,47] in the corresponding calculations. It is obvious that we need to face this puzzle in this channel. More experimental and theoretical efforts are needed to clarify this point.

$K_2(1770)$ and $K_2(1820)$ satisfy

$$\begin{pmatrix} |K_2(1770)\rangle \\ |K_2(1820)\rangle \end{pmatrix} \approx \begin{pmatrix} \cos\theta_{1D} & \sin\theta_{1D} \\ -\sin\theta_{1D} & \cos\theta_{1D} \end{pmatrix} \begin{pmatrix} |1^1D_2\rangle \\ |1^3D_2\rangle \end{pmatrix}. \quad (43)$$

According to Fig. 6, we find that $K_2(1770)$ mainly decays to $K_2^*(1430)\pi$, $K^*\pi$, $K\pi$, and $K\omega$. Experiments show that $K_2^*(1430)\pi$ is the dominant decay mode of $K_2(1770)$ [1], which indicates that θ_{1D} favors the value less than zero.

$K_3^*(1780)$ together with $\rho_3(1690)$, $\omega_3(1670)$, and $\phi_3(1850)$ forms a 1^3D_3 nonet. We give it a mass of 1.781 GeV by the MGI model, which is consistent with the experimental data of 1.776 GeV. As shown in Table 9, even though $K^*\rho$ is the dominant decay mode of $K_3^*(1780)$, it is not observed in experiments so far. The channel $K^*\omega$ has a sizable contribution to its total decay width, which is still missing in experiment. A final state $K\pi$ largely contributes to the total width and theory and experiments are consistent. The branching ratio $\Gamma_{K^*\pi}/\Gamma_{K\pi}$ agrees with the experimental data [70].

Next, let us focus on $K_2(1820)$. According to Fig. 7, one notices that $K_2(1820)$ probably decays to $K\pi\pi$, $K_2^*(1430)\pi$, $Kf_2(1270)$, $K^*\pi$, and $K\omega$, in which $K\pi\pi$ comes from $K\rho$ channel. As seen from the θ_{1D} dependence of the widths of $K_2(1820)$ in Fig. 7, we notice that contributions of $K\rho$ and $Kf_2(1270)$ are large when $\theta_{1D} < 0$, which indicates that it is very likely that θ_{1D} is smaller than zero, which is consistent with the previous analysis for $K_2(1770)$. Because of the absence of the experimental information, we cannot confirm the angle θ_{1D}, while our results will be helpful for the future experiments to study this state.

4.3.2 2D states

As one of the 2D states is missing, using the familiar program with 2P states, we obtain

$$\begin{pmatrix} |K_2(1990)\rangle \\ |K_2(2250)\rangle \end{pmatrix} \approx \begin{pmatrix} \cos\theta_{2D} & \sin\theta_{2D} \\ -\sin\theta_{2D} & \cos\theta_{2D} \end{pmatrix} \begin{pmatrix} |2^1D_2\rangle \\ |2^3D_2\rangle \end{pmatrix}, \quad (44)$$

where $K_2(1990)$ is obtained from an equation similar to Eq. (42).

According to Table 10, one finds that $K_2(2250)$ as a $2D'$ state mainly decays into $Ka_2(1700)$, $K_2^*(1980)\pi$, $K_3^*(1780)\pi$, $K^*(1410)\pi$, and $K_2^*\pi$. $K_2^*\pi$ and $Kf_2(1270)$ have been observed in experiments which have sizable contributions to the total width. Besides, $K\rho$, which is an important decay channel in our result, can decay into $K\pi\pi$, which is observed in experiment. On the other hand, the theoretical total width is larger than the experimental value 180 MeV given in PDG. We need more experimental information to study this $2D'$ state, to test our results, and to have more detailed decay widths to ascertain the value of θ_{2D}.

We use 1994 MeV as the mass of the partner of $K_2(2250)$ with $\theta_{2D} \approx \pm44°$, and calculate the strong decay of this state as shown in Table 11. According to this table, we can find that its main decay channels are $K^*\pi$, $K\rho$, $K_2^*\pi$, and $K_3^*(1780)\pi$.

Table 9 The decay widths of the 1^3D_1 and 1^3D_3 states. Here, $K^*(1680)$ and $K_3^*(1780)$ are assigned to be the pure 1^3D_1 state and 1^3D_3 states, respectively. The unit of the width is MeV

State	Channel	This work	Ref. [3]	Experiment
1^3D_1	$K\pi$	69.2	45	–
	$K^*\pi$	41.8	25	–
	$K\rho$	44.7	26	–
	$K\eta$	64.4	53	–
	$K^*\rho$	6.33	2	–
	$K^*\omega$	1.69	1	–
	Kh_1	78	33	–
	$K_1(1270)\pi$	330	145	–
	$K_1(1400)\pi$	7.86	0	–
	$K\phi$	9.35	45	–
	Total	653	348	$426 \pm 18 \pm 30$ [58]
	$\Gamma_{K\pi}/\Gamma_{K^*\pi}$	1.66	1.8	2.8 ± 1.1 [71]
	$\Gamma_{K\rho}/\Gamma_{K\pi}$	0.65	0.58	1.2 ± 0.4 [71]
	$\Gamma_{K\rho}/\Gamma_{K^*\pi}$	1.07	1.04	$1.05^{+0.27}_{-0.11}$
1^3D_3	$K^*\rho$	118	42	–
	$K\rho$	20.1	10	74 ± 10 [47]
	$K^*\omega$	36.4	12	–
	$K\pi$	38.1	40	31.7 ± 3.7 [47]
	$K^*\pi$	28.5	14	45 ± 7 [47]
	$K\omega$	6.45	3	–
	$K\eta$	9.67	19	48 ± 21 [1], 15 ± 6 [72]
	$K_1(1270)\pi$	1.68	1	–
	$K_1(1400)\pi$	2.80	1	–
	$K_2^*(1430)\pi$	4.18	1	< 25 [72]
	Total	266	145	225 ± 60 [73]
	$\Gamma_{K\rho}/\Gamma_{K^*\pi}$	0.702	0.71	1.52 ± 0.23 [70]
	$\Gamma_{K^*\pi}/\Gamma_{K\pi}$	0.748	0.35	1.09 ± 0.26 [70]
	$\Gamma_{K\eta}/\Gamma_{K\pi}$	0.253	0.48	1.6 ± 0.7 [1]
	$\Gamma_{K\pi}/\Gamma_{\text{Total}}$	0.143	0.28	0.188 ± 0.010 [1]
	$\Gamma_{K\rho}/\Gamma_{\text{Total}}$	7.5%	6.9%	$(31 \pm 9)\%$ [1]
	$\Gamma_{K^*\pi}/\Gamma_{\text{Total}}$	10.7%	9.7%	$(20 \pm 5)\%$ [1]
	$\Gamma_{K\eta}/\Gamma_{\text{Total}}$	3.6 %	13%	$(30 \pm 13)\%$ [1]

4.4 F-wave kaons

4.4.1 $1F$ states

In this section, we discuss possibility of different assignments of $K_2^*(1980)$ from two aspects, mass and decay information. In 1987, LASS reported a structure in the reaction $K^-p \to \bar{K}^0\pi^+\pi^-n$ [64], and they obtained the resonance parameters $M = (1973 \pm 8 \pm 25)$ MeV and $\Gamma = (373 \pm 33 \pm 60)$ MeV. This is the particle called $K_2^*(1980)$ listed in PDG [1]. Barnes et al. [3] have the viewpoint that $K_2^*(1980)$ is a 1^3F_2 state, and they give a total width of 300 MeV. On the other hand, our results show that the mass of a 1^3F_2 state is about 2093 MeV. Ebert et al. [4] predict a 1^3F_2 state with a mass of 1964 MeV. As the partner of an iso-vector of 1^3F_2,

$a_2(2030)$ is well established in Ref. [32]. In the same nonet, the meson which contains one s quark is probably heavier than the mesons which only contain u/d quarks. Along this line, the mass of the 1^3F_2 state of the kaon should be larger than 2030 MeV, so that the mass $K_2^*(1980)$ is a bit small as a 1^3F_2 state. References [2–4] and this work give the mass for a 2^3P_2 state 1938, 1896, 1850, and 1870 MeV, respectively, and for its iso-vector partner, $a_2(1700)$ [32], the mass of $K_2^*(1980)$ is a bit larger as a 2^3P_2 state. We should, of course, combine the decay information of $K_2^*(1980)$ to determine which possibility for its assignment we should take.

Both Ref. [3] and this work (see Table 7) show that $K_1(1270)\pi$ is the dominant decay channel when we treat $K_2^*(1980)$ as a 1^3F_2 state, even though the channel is not observed in experiments. $K_2(1770)\pi$, Kb_1, Ka_1, $K\pi$, $K\rho$,
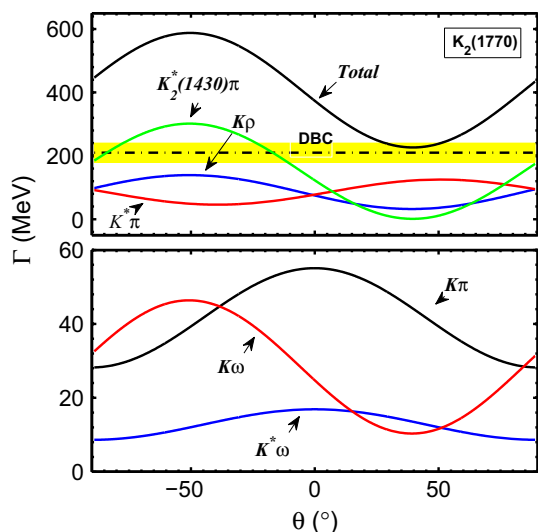
Fig. 6 θ_{1D} dependence of the width of $K_2(1770)$, where the dot-dashed line is the experimental value of DBC [69]
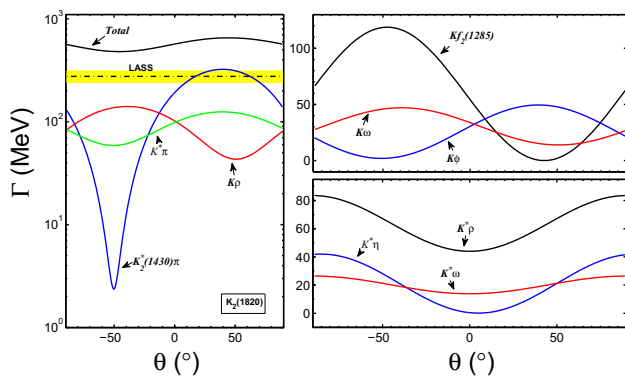

Fig. 7 θ_{1D} dependence of the decay width of $K_2(1820)$. Here a dot-dashed line LASS with a yellow band is taken from [64]

and $K^*\pi$ modes, among which $K\rho$ and $K^*\pi$ have been reported in the experiment [1], also have sizable contributions, where we take $\theta_{1D} = -39°$. If $K_2^*(1980)$ is a 1^3F_2 state, our prediction for the channels $K_1(1270)\pi$, $K_2(1770)\pi$, Kb_1, Ka_1, and $K\pi$ will be helpful for the experiment to test this assignment.

Both Ref. [3] and our results show that $K_2^*(1980)$ is 2^3P_2 state, where Ref. [3] takes the mass to be 1850 MeV and we take an experimental value of 1973 MeV. For this reason, the results between their and this work show some difference. The main decay modes are $K^*\rho$, $K\pi$, $K^*\pi$, $K\rho$, $K^*\eta$, $K\eta'$, and $K^*\omega$. Besides $K\rho$ and $K^*\pi$, one notices that Kf_2 has been observed in experiments which has sizable contributions in theory. Hence $K_2^*(1980)$ to be assigned to 2^3P_2 is also reasonable.

Finally, let us draw a rough conclusion for $K_2^*(1980)$. According to the mass analysis, the mass of $K_2^*(1980)$ is a bit small when assigned to a 1^3F_2 state and a bit large when

assigned to a 2^3P_2 state. According to the decay information, $K_2^*(1980)$ is in favor of a 2^3P_2 state. We still, however, need more experimental information to test our assignment for $K_2^*(1980)$. What is more important is that we give the prediction that the partial widths of $K_2^*(1425)\pi$, $K^*(1410)\pi$, $K^*\omega$, $K^*\rho$, and $K^*\eta$ treating $K_2^*(1980)$ as 1^3F_2 will be much larger than those of the case of a 2^3P_2 state. The experimental study of these decay modes combined with our prediction will help us to determine the assignment of $K_2^*(1980)$. Besides the above, our prediction can help future experiments to find the missing 1^3F_2 or 2^3P_2 state. According to Table 3, one can notice that our spectral results are consistent with the mass of $K_4^*(2045)$ given by PDG when we treat it as 1^3F_4 state. As for the strong decay of $K_4^*(2045)$, one can notice that both the results of Ref. [3] and this work (Table 12) show that $K^*\rho$, $K\pi$, $K^*\pi$, $K^*\omega$, and $K\rho$ are the main decay channels. The PDG gives two partial width ratios: one is $\Gamma_{K\pi}/\Gamma_{Total} = (9.9 \pm 1.2)\%$ and our result is $\Gamma_{K\pi}/\Gamma_{Total} = 8.4\%$, which is consistent with the experiment. Another is $\Gamma_{K^*\phi}/\Gamma_{Total} = (1.4 \pm 0.7)\%$ and we obtain $\Gamma_{K^*\phi}/\Gamma_{Total} = 1.54\%$, which is consistent with the experiment as well. On the other hand, Ref. [3] obtained 21 and 3.1% for these two partial width ratios, which are different from the experiment. These results, of course, prove the superiority of the accurate meson wave functions we have obtained.

References [2–4] and this work give the mass of a $1F$ state 2131, 2009, 2050, and 2075 MeV (which we call $K_3(2075)$, and strictly speaking, this state is a pure 1^1F_3 state, here we assume the physical state $1F$ has this mass), respectively, among which one notices that the last two results are almost identical. $K_3(2075)$ is assigned to the missing $1F$ state. We present the θ_{nF} dependence of the widths for these two cases in Table 13. The total width of a $1F$ state with a mass of 2075 MeV is about (400–600) MeV, which means that the predicted $K_3(2075)$ is a broad state and it is not easy to identify $K_3(2075)$ in experiments. Its main decay channels are $K_3^*(1780)\pi$, $K^*\rho$, $K^*\pi$, Ka_2, $K\rho$ and $K_2^*\pi$.

4.4.2 2F states

$K_3(2F)$ and $K_3(2F')$ mixing satisfies

$$\begin{pmatrix} |K_3(2320)\rangle \\ |K_3(2360)\rangle \end{pmatrix} \approx \begin{pmatrix} \cos\theta_{2F} & \sin\theta_{2F} \\ -\sin\theta_{2F} & \cos\theta_{2F} \end{pmatrix} \begin{pmatrix} |2^1F_3\rangle \\ |2^3F_3\rangle \end{pmatrix}, \quad (45)$$

where $K_3(2360)$ is obtained from an equation similar to Eq. (42). The total width of $K_3(2320)$ is nearly (180–200) MeV, which is consistent with the data of OMEG (150 ± 30) MeV [75]. $K_3(2320)$ mainly decays to $K_3^*(1780)\pi$, $K^*(1410)\pi$, $K\rho$ and $K^*\pi$. The total width of $K_3(2360)$ is nearly (80–120) MeV. $K_3(2360)$ mainly decays to $K_3^*(1780)\pi$, $K\rho_3(1690)$, $K\rho$ and $K^*\pi$, which are given in

Table 10 Strong decay information of $K_2(2250)(2D')$, where s and c represent sine and cosine functions. The unit of the width is MeV

Decay channel	Width	Decay channel	Width
Total	$956c^2 - 267cs + 1044s^2$	$Ka_2(1700)$	$115c^2 - 188cs + 77.1s^2$
$K_2^*(1980)\pi$	$82.6c^2 - 136cs + 57.4s^2$	$K_3^*(1780)\pi$	$67.3c^2 - 135cs + 71.4s^2$
$K^*(1410)\pi$	$75.5s^2 + 55.6c^2 - 97.2cs$	$K_2^*\pi$	$58.9c^2 - 70.9cs + 64.2s^2$
Ka_2	$52.9c^2 - 57cs + 55.1s^2$	$K\rho_3(1690)$	$33.7c^2 - 64.5cs + 31s^2$
$K^*\pi$	$31.3c^2 - 50.3cs + 21.1s^2$	$K\rho(1450)$	$42.4c^2 - 23.3cs + 37.6s^2$
$K\rho$	$29.7c^2 - 48cs + 19.9s^2$	K^*a_2	$9.24c^2 - 30.9cs + 37.9s^2$
$K^*(1410)\rho$	$22.1c^2 + 42.1s^2$	$K^*\pi(1300)$	$25.6c^2 - 40.4cs + 17.3s^2$
$K^*\rho$	$37.7c^2 + 40.2s^2$	$K_1(1400)\rho$	$15.5c^2 - 42.8cs + 16.7s^2$
$K\omega_3(1670)$	$15.1c^2 - 29cs + 14s^2$	Kf_2	$19.9c^2 - 18.1cs + 20.1s^2$
$Kf_2'(1525)$	$19.9c^2 - 18.1cs + 20.1s^2$	$K_2^*\omega$	$3.49c^2 - 12.9cs + 15.6s^2$
$K\omega$	$9.85c^2 - 15.9cs + 6.61s^2$	K^*b_1	$14.3c^2 - 0.4cs + 16.1s^2$
K^*a_1	$6.74c^2 - 7cs + 14.1s^2$	$Ka_0(1450)$	$4.36c^2 - 13.7cs + 10.8s^2$
$K\omega(1420)$	$14.1c^2 - 2.21cs + 13.6s^2$	$K^*\eta$	$0.101c^2 - 0.517cs + 14.2s^2$
$K^*\omega$	$12.5c^2 + 13.2s^2$	$K^*(1410)\omega$	$6.37c^2 + 12.3s^2$
K^*h_1	$10.2c^2 - 3.25cs + 10.6s^2$	K^*f_2	$6.31c^2 - 7.46cs + 9.34s^2$
$K^*(1680)\pi$	$4.98c^2 - 11cs + 6.44s^2$	$K^*\eta(1295)$	$0.0195c^2 - 0.914cs + 10.7s^2$
$K^*\phi$	$8.35c^2 + 6.81s^2$	$K_1(1400)\omega$	$1.26c^2 - 1.09cs + 8.18s^2$

Table 11 The main strong decay widths of $K_2(1990)$ as an $2D$ state, where s and c represent sine and cosine functions. The unit of the width is MeV

Decay channel	Width
Total	$97.9c^2 - 17.3cs + 120s^2$
$K^*\pi$	$15.1c^2 - 22cs + 19.6s^2$
$K\rho$	$12.5c^2 + 19.2cs + 16.4s^2$
$K_2^*\pi$	$17.9c^2 - 16.5cs + 7.59s^2$
$K_3^*(1780)\pi$	$7.16c^2 - 14.4cs + 7.26s^2$

Table 12 The strong decay widths of $K_4^*(2045)$ assigned to a 1^3F_4 state. The unit of the width is MeV

State	Channel	This work	Ref. [3]	Experiment
$K_4^*(2045)$ (1^3F_4)	$K^*\rho$	84.9	29	–
	$K\rho$	16.1	7	–
	$K^*\omega$	27.7	9	–
	$K\omega$	5.24	2	–
	$K\pi$	21.0	21	–
	$K^*\pi$	20.5	8	–
	$K^*(1410)\pi$	2.91	0	–
	$K_1(1270)\pi$	11.4	2	–
	$K_1(1400)\pi$	6.47	2	–
	$K\phi$	0.783	1	–
	Ka_1	4.17	1	–
	Ka_2	13.5	1	–
	Kb_1	13.0	2	–
	$K^*\phi$	3.84	3	–
	$K_2^*(1430)\pi$	15.9	2	–
	$K_1(1270)\eta$	3.13	1	–
	Total	250	98	198 ± 30
	$\Gamma_{K\pi}/\Gamma_{\text{Total}}$	8.40%	21%	$9.9 \pm 1.2\%$ [58]
	$\Gamma_{K^*\phi}/\Gamma_{\text{Total}}$	1.54%	3.1%	$1.4 \pm 0.7\%$ [74]

Table 14. Although we cannot give the mixing angle of these two states for lack of experimental information, our theoretical results can be helpful for studying these two states in future experiments.

4.5 G-wave kaons

4.5.1 $1G$ states

$K_4(1G)$ and $K_4(1G')$ mixing satisfies

$$\begin{pmatrix} |K_4(2310)\rangle \\ |K_4(1G')\rangle \end{pmatrix} \approx \begin{pmatrix} \cos\theta_{1G} & \sin\theta_{1G} \\ -\sin\theta_{1G} & \cos\theta_{1G} \end{pmatrix} \begin{pmatrix} |1^1G_4\rangle \\ |1^3G_4\rangle \end{pmatrix}. \quad (46)$$

We assume the mass of a $1G$ state to be about 2309 MeV, which we call $K_4(2310)$. The GI model [2] and Ref. [4] give this mass values of 2422 and 2255 MeV, respectively, while the mass of the K_4 state in PDG is 2490 MeV. According to Table 3, $K_4(2500)$ may be a $2G$ state. We predict the

strong decay information of these two G wave states in Table 15.

As shown in Table 15, main decay modes of $K_4(2310)$ are $K_4^*(2045)\pi$, $K_3^*(1780)\pi$, $K\rho_3(1690)$, Ka_2 and $K_2^*\pi$ when $K_4(2310)$ is assigned to a $1G$ state. Its total width will

Table 13 Strong decay information of $K_3(2320)$ as an $2F$ state and (predicted) $K_3(2075)(1F)$ depending on their mixing angle, where s and c represent sine and cosine functions. The unit of the width is MeV

Decay channel	$K_3(2075)$ as $1F$ state	$K_3(2320)$ as $2F$ state
Total	$464c^2 + 182cs + 530s^2$	$189c^2 + 21.2cs + 202s^2$
$K_3^*(1780)\pi$	$107c^2 + 245cs + 141s^2$	$24c^2 + 42.4cs + 21.3s^2$
$K^*(1410)\pi$	$6.93c^2 + 0.975cs + 7.07s^2$	$20.3c^2 + 27.2cs + 16.4s^2$
$K\rho$	$38.7c^2 + 11.1cs + 40.3s^2$	$11c^2 + 20.4cs + 13.9s^2$
$K^*\pi$	$40.5c^2 + 4.03cs + 39.9s^2$	$10.4c^2 + 20.2cs + 13.3s^2$
$Ka_2(1700)$	0	$12.9c^2 + 13.7cs + 9.98s^2$
$K_2^*(1980)\pi$	0	$11.5c^2 + 12.3cs + 8.81s^2$
$K\rho_3(1690)$	0	$8.44c^2 + 16.2cs + 8.19s^2$
$K^*(1410)\rho$	0	$13.5c^2 + 9.77s^2$
$K^*\rho$	$55.7c^2 + 43.7s^2$	$12.3c^2 + 8.63s^2$
$K\rho(1450)$	$1.51c^2 + 3.33cs + 1.99s^2$	$7.87c^2 + 1.95cs + 8.15s^2$
$K\omega_3(1670)$	0	$4.04c^2 + 7.94cs + 4.13s^2$
$K^*(1410)\eta$	$0.0642c^2 + 0.408cs + 0.703s^2$	$0.163c^2 + 0.557cs + 7.7s^2$
$K\omega$	$12.8c^2 + 4.01cs + 13.3s^2$	$3.63c^2 + 6.79cs + 4.61s^2$
$K^*\pi(1300)$	0	$3.56c^2 + 6.55cs + 4.51s^2$
$K_4^*(2045)\pi$	0	$4.3c^2 + 4.62cs + 1.56s^2$
$K(1460)\rho$	0	$2.41c^2 + 5.2cs + 3.16s^2$
$K^*(1680)\pi$	$0.248c^2 + 1.02cs + 1.05s^2$	$3.33c^2 + 4.79cs + 1.73s^2$
$K_2^*\rho$	0	$3.96c^2 + 1.4cs + 3.94s^2$
$K^*(1410)\omega$	0	$4.14c^2 + 2.97s^2$
$K^*\omega$	$18.1c^2 + 14.2s^2$	$4c^2 + 2.83s^2$
$Ka_0(1450)$	$1.15c^2$	$3.91c^2$
K^*a_2	0	$2.73c^2 + 0.957cs + 2.7s^2$
$K\omega(1420)$	$0.93c^2 + 1.94cs + 1.21s^2$	$2.89c^2 + 0.472cs + 2.82s^2$
$K^*\eta$	$0.106c^2 + 1.54cs + 15.4s^2$	$0.0206c^2 + 0.429cs + 2.86s^2$
Ka_2	$50.3c^2 + 54.7cs + 37.3s^2$	$1.84c^2 + 2.13cs + 0.972s^2$
Ka_1	$24.5s^2$	$2.33s^2$
Kb_1	$6.76s^2$	$2.07s^2$
$K_0^*(1945)\pi$	0	$1.66c^2$
$K\phi$	$6.29c^2 + 10.4cs + 7.78s^2$	$0.787c^2 + 1.33cs + 0.98s^2$
$K_2^*\omega$	0	$1.28c^2 + 0.452cs + 1.28s^2$
Kf_2	$20c^2 + 14.6s^2 + 21.9cs$	$1.03c^2 + 1.05cs + 0.123s^2$
$K_2^*\pi$	$55.5c^2 + 60.8cs + 40.4s^2$	$0.742c^2 + 0.853cs + 0.366s^2$
$K_2^*\eta$	$8.55c^2 + 1.11cs + 0.0976s^2$	$0.773c^2 + 0.0199cs + 0.000205s^2$
$K^*\phi$	$3.01c^2 + 2.04s^2$	$0.474c^2 + 0.585s^2$
$K^*\eta'$	$2.7c^2 + 1.74cs + 0.309s^2$	$0.429c^2 + 0.206cs + 0.0584s^2$
$K_1(1270)\rho$	$5.65c^2 + 5.95cs + 5.16s^2$	$0.263c^2 + 0.216cs + 0.268s^2$
$Kf_1(1420)$	$2.93s^2$	$0.0280c^2 + 0.366s^2$
Kh_1	$2.89s^2$	$0.198c^2 + 0.347s^2$
Kf_1	$6.98s^2$	$0.136c^2 + 0.225s^2$

Table 14 The main strong decay widths of $K_3(2360)$ assigned to an $2F'$ state, where s and c represent sine and cosine functions. The unit of the width is MeV

Decay channel	Width
Total	$93c^2 + 34cs + 101s^2$
$K_3{}^*(1780)\pi$	$28.3c^2 + 54.7cs + 30.4s^2$
K $\rho_3(1690)$	$16c^2 - 22.8cs + 22.8s^2$
K ρ	$15.1c^2 - 20.3cs + 12.1s^2$
$K^*\pi$	$14.3c^2 + 20cs + 11.4s^2$
$K_4{}^*(2045)\pi$	$2.52c^2 + 11.9cs + 11.4s^2$
K $\omega_3(1670)$	$6.88c^2 - 9.62cs + 9.62s^2$
$K^*\rho$	$9.83c^2 + 14.3s^2$

be (710–880) MeV, which is not easy to observe in experiments.

4.5.2 2G states

$K_4(2500)$ and its partner $K_4(2550)$ (predicted) satisfy

$$\begin{pmatrix} |K_4(2500)\rangle \\ |K_4(2550)\rangle \end{pmatrix} \approx \begin{pmatrix} \cos\theta_{2G} & \sin\theta_{2G} \\ -\sin\theta_{2G} & \cos\theta_{2G} \end{pmatrix} \begin{pmatrix} |2^1G_4\rangle \\ |2^3G_4\rangle \end{pmatrix}, \quad (47)$$

where $K_4(2550)$ is obtained from an equation similar to Eq. (42).

The total width of $K_4(2500)$ assigned to a $2G$ state is about (230–290) MeV, which is consistent with the experimental value ~250 MeV [76]. According to Table 15, the main decay channels of $K_4(2500)$ are $K_3^*(1780)\pi$, $K\rho_3(1690)$, Ka_2, $K_2^*\pi$, $K_4^*(2045)\pi$, K^*b_1, $K_2^*(1980)\pi$ and $K\omega_3(1670)$, etc. Information of these predicted decay widths is important to study the mixing angle of this state for future experiments.

The total width of $K_4(2550)$ assigned to a $2G'$ state is about (230–260) MeV. According to Table 16, the main decay channels of $K_4(2550)$ are $K_3^*(1780)\pi$, $K\rho_3(1690)$, Ka_2, $K_4^*(2045)\pi$, $K_2^*(1980)\pi$ and K^*b_1, etc. We hope our prediction can be helpful for the future experiment to study these two states and their mixing angle.

Table 15 The widths of (predicted) $K_4(2310)$ and $K_4(2500)$ depending on their mixing angle, where s and c represent sine and cosine functions. The unit of the width is MeV

Decay channels	Width ($K_4(2310)$ assigned to 1G state)	Width ($K_4(2500)$ assigned to 2G state)
Total	$664c^2 + 31cs + 754s^2$	$222c^2 + 7.5cs + 247s^2$
$K_4^*(2045)\pi$	$90.2c^2 + 201cs + 112s^2$	$14.6c^2 + 28.7cs + 14.6s^2$
$K_3^*(1780)\pi$	$80c^2 + 168cs + 92.3s^2$	$21.6c^2 + 44.1cs + 24.7s^2$
$K\rho_3(1690)$	$63.1c^2 + 140.cs + 77.6s^2$	$19c^2 + 41.6cs + 23.3s^2$
Ka_2	$43.1c^2 + 70.4cs + 40.9s^2$	$17.5c^2 + 34.cs + 20.5s^2$
$K_2^*\pi$	$41.7c^2 + 62.6cs + 38.6s^2$	$16.7c^2 + 31.7cs + 20.2s^2$
$K\omega_3(1670)$	$24c^2 + 52.8cs + 29.2s^2$	$7.11c^2 + 15.5cs + 8.69s^2$
K^*b_1	$22.2c^2 + 45.2cs + 27.1s^2$	$8.14c^2 + 17.2cs + 10.s^2$
$K^*\rho$	$29.9c^2 + 28.2s^2$	$9.16c^2 + 7.28s^2$
$K^*\pi$	$19c^2 + 15cs + 17.3s^2$	$7.05c^2 + 3.28cs + 7.42s^2$
Kf_2	$15.2c^2 + 22.3cs + 13.3s^2$	$6.22c^2 + 11.7cs + 7.08s^2$
K^*a_1	$10.9c^2 + 22.5cs + 12.9s^2$	$4.18c^2 + 8.74cs + 5.1s^2$
K^*h_1	$10.8c^2 + 20.2cs + 12.9s^2$	$3.74c^2 + 7.88cs + 4.6s^2$
$K\rho$	$17.5c^2 + 7.35cs + 16.7s^2$	$7.76c^2 + 4.cs + 8.21s^2$
K^*a_2	$15.4c^2 + 11.5cs + 9.12s^2$	$5.58c^2 + 3.68cs + 4.01s^2$
$K_2^*\rho$	$14.9c^2 + 11.2cs + 8.83s^2$	$3.36c^2 + 2.39cs + 2.96s^2$
$K_2^*\eta$	$0.241c^2 + 3.62cs + 17.1s^2$	$0.139c^2 + 0.96cs + 2.35s^2$
$K^*(1410)\pi$	$10.2c^2 + 7.29cs + 9.41s^2$	$4.39c^2 + 7.83cs + 3.51s^2$
Ka_1	$3.07c^2 + 11.1cs + 9.99s^2$	$1.19c^2 + 2.63cs + 1.46s^2$
K^*f_2	$9.84c^2 + 7.37cs + 5.98s^2$	$3.04c^2 + 1.99cs + 2.07s^2$
$K^*\omega$	$9.79c^2 + 9.18s^2$	$3.0c^2 + 2.38s^2$
$K\rho(1450)$	$5.22c^2 + 7.23cs + 6.02s^2$	$0.95c^2 + 1.67cs + 0.764s^2$
$K\omega$	$5.77c^2 + 2.3cs + 5.51s^2$	$2.55c^2 + 1.38cs + 2.71s^2$
$K^*(1680)\pi$	$2.31c^2 + 6.41cs + 4.45s^2$	$0.439c^2 + 0.2cs + 0.0385s^2$
$K_2^*\omega$	$4.35c^2 + 3.26cs + 2.57s^2$	$0.01c^2 + 0.724cs + 0.909s^2$
$K_0^*(1430)\pi$	$2.3c^2 + 5.12cs + 2.84s^2$	$0.0247c^2 + 0.232cs + 0.546s^2$
$K_2^*(1980)\pi$	$1.43c^2 + 3.14cs + 1.76s^2$	$9.02c^2 + 16.7cs + 9.55s^2$
$K\phi$	$1.92c^2 + 2.01cs + 2.14s^2$	$0.36c^2 + 0.771cs + 0.446s^2$
Kb_1	$3.02s^2$	$0.988s^2$
$K^*\phi$	$2.08c^2 + 1.67s^2$	$0.247c^2 + 0.198s^2$
$K^*(1410)\eta$	$1.4c^2 + 0.694cs + 0.209s^2$	$1.82c^2 + 0.611cs + 0.0524s^2$
$K^*(1410)\rho$	$1.03c^2 + 0.79s^2$	$6.55c^2 + 6.31s^2$

5 Conclusions and discussion

In this paper, we have given the analysis of the mass spectra of the kaon family via the modified Godfrey–Isgur quark model that includes a color screening effect, and we have obtained the structure information of the observed kaon candidates. Then we have further tested the possible assignments by comparing the theoretical results of their two-body strong decays with the experimental data. Additionally, we have also predicted the behaviors of some partial decay widths of the

kaons, which are still missing in experiments. In Table 17, we summarize the mass and main decay modes of these states, by which experiment may carry out the search for them.

This study is crucial to establish the kaon family and future search for their higher excitations. We have discussed the possible assignments to the kaons listed in PDG. The main task of the present work has been a calculation of the spectra and OZI-allowed two-body strong decays of the kaon family, which can test the possible assignments to the kaons. In

Table 16 The strong decay widths of $K_4(2550)$ assigned to a $2G'$ state, where s and c represent sine and cosine functions. The unit of the width is MeV

Decay channel	Width
Total	$238c^2 + 38cs + 218s^2$
$K_3^*(1780)\pi$	$32.7c^2 + 57.5cs + 28.3s^2$
$K\rho_3(1690)$	$31.2c^2 - 55.3cs + 25.7s^2$
$K_4^*(2045)\pi$	$25.1c^2 + 48.1cs + 24s^2$
Ka_2	$21.8c^2 - 35.8cs + 19.8s^2$
$K_2^*\pi$	$23c^2 + 34.8cs + 19.4s^2$
K^*b_1	$15.1c^2 + 25.8cs + 12.3s^2$
$K\omega_3(1670)$	$10.9c^2 - 19.3cs + 9.05s^2$
$K\rho$	$9.72c^2 - 1.24cs + 9.58s^2$
K^*a_2	$7.94c^2 - 7.73cs + 11.9s^2$
K^*a_1	$5.90c^2 + 6.60cs + 4.95s^2$
$K_2^*\rho$	$6.29c^2 + 5.64cs + 8.34s^2$

Table 17 The mass and the important strong decay channels for some predicted kaon states which can be helpful in future search for them in experiments. The units of the mass and width are MeV

State	Assignment	Mass	Main decay channels
$K_1(2030)$	$2P'$	~ 2030	$K^*\pi$, $K\rho$
$K_2(1990)$	$2D$	~ 1994	$K^*\pi$, $K\rho$
$K_3(2075)$	$1F$	~ 2075	$K_3^*(1780)\pi$, $K^*\rho$
$K_3(2360)$	$2F'$	~ 2362	$K_3^*(1780)\pi$, $K\rho_3(1690)$
$K_4(2310)$	$1G$	~ 2309	$K_4^*(2045)\pi$, $K_3^*(1780)\pi$
$K_4(2550)$	$2G'$	~ 2550	$K_3^*(1780)\pi$, $K\rho_3(1690)$

Sects. 2 and 3, we have discussed these points in detail. The predicted decay behaviors of the discussed kaons can provide valuable information for further experimental study in the future.

At present, experimental information on the kaons is not abundant. Thus, we suggest to do more experimental measurements of the resonance parameters and to search for the missing main decay channels. Such an effort will be not only helpful to establish the kaon family in experiments, but it is also valuable to study the production of hidden-charm pentaquarks $P_c(4380)$ and $P_c(4450)$ by analyzing $\Lambda_b \rightarrow J/\psi p K$ [77], which has a close relation to the understanding of the kaon family. With experimental progress, the exploration of the kaons will become a major issue in hadron physics, we have been provided good platforms in the BESIII, BelleII, and COMPASS experiments. We hope that, inspired by this work, more experimental and theoretical studies of high-spin states are conducted in the future.

References

1. K.A. Olive et al., Particle Data Group. Chin. Phys. C **38**, 090001 (2014)
2. S. Godfrey, N. Isgur, Phys. Rev. D **32**, 189 (1985)
3. T. Barnes, N. Black, P.R. Page, Phys. Rev. D **68**, 054014 (2003). arXiv:nucl-th/0208072 [nucl-th]
4. D. Ebert, R. Faustov, V. Galkin, Phys. Rev. D **79**, 114029 (2009). arXiv:0903.5183 [hep-ph]
5. Q.-T. Song, D.-Y. Chen, X. Liu, T. Matsuki, Phys. Rev. D **91**, 054031 (2015a). arXiv:1501.03575 [hep-ph]
6. Q.-T. Song, D.-Y. Chen, X. Liu, T. Matsuki, Phys. Rev. D **92**, 074011 (2015b). arXiv:1503.05728 [hep-ph]
7. L. Micu, Nucl. Phys. B **10**, 521 (1969)
8. A. Le Yaouanc, L. Oliver, O. Pene, J. Raynal, Phys. Rev. D **8**, 2223 (1973)
9. E. van Beveren, C. Dullemond, G. Rupp, Phys. Rev. D **21**, 772 (1980) [**Erratum: Phys. Rev. D 22, 787 (1980)**]
10. E. van Beveren, G. Rupp, T. Rijken, C. Dullemond, Phys. Rev. D **27**, 1527 (1983)
11. A. Le Yaouanc, L. Oliver, O. Pene, J.C. Raynal, *Hardron Transitions In The Quark Model* (Gordon and Breach, New York, 1988)
12. W. Robertsand, B. Silvestre-Brac, Acta Phys. Austriaca **11**, 171 (1992)
13. S. Capstickand, W. Roberts, Phys. Rev. D **49**, 4570 (1994). arXiv:nucl-th/9310030 [nucl-th]
14. H.G. Blundelland, S. Godfrey, Phys. Rev. D **53**, 3700 (1996). arXiv:hep-ph/9508264 [hep-ph]
15. E. Ackleh, T. Barnes, E. Swanson, Phys. Rev. D **54**, 6811 (1996). arXiv:hep-ph/9604355 [hep-ph]
16. S. Capstickand, B. Keister. arXiv:nucl-th/9611055 [nucl-th]
17. R. Bonnaz, B. Silvestre-Brac, C. Gignoux, Eur. Phys. J. A **13**, 363 (2002). arXiv:hep-ph/0101112 [hep-ph]
18. F. Closeand, E. Swanson, Phys. Rev. D **72**, 094004 (2005). arXiv:hep-ph/0505206 [hep-ph]
19. B. Zhang, X. Liu, W.-Z. Deng, S.-L. Zhu, Eur. Phys. J. C **50**, 617 (2007). arXiv:hep-ph/0609013 [hep-ph]
20. J. Lu, X.-L. Chen, W.-Z. Deng, S.-L. Zhu, Phys. Rev. D **73**, 054012 (2006). arXiv:hep-ph/0602167 [hep-ph]
21. Z.-F. Sunand, X. Liu, Phys. Rev. D **80**, 074037 (2009). arXiv:0909.1658 [hep-ph]
22. X. Liu, Z.-G. Luo, Z.-F. Sun, Phys. Rev. Lett. **104**, 122001 (2010). arXiv:0911.3694 [hep-ph]
23. Z.-F. Sun, J.-S. Yu, X. Liu, T. Matsuki, Phys. Rev. D **82**, 111501 (2010). arXiv:1008.3120 [hep-ph]
24. T. Rijken, M. Nagels, Y. Yamamoto, Nucl. Phys. A **835**, 160 (2010)
25. J.-S. Yu, Z.-F. Sun, X. Liu, Q. Zhao, Phys. Rev. D **83**, 114007 (2011). arXiv:1104.3064 [hep-ph]
26. Z.-Y. Zhouand, Z. Xiao, Phys. Rev. D **84**, 034023 (2011). arXiv:1105.6025 [hep-ph]

27. Z.-C. Ye, X. Wang, X. Liu, Q. Zhao, Phys. Rev. D **86**, 054025 (2012). arXiv:1206.0097 [hep-ph]
28. X. Wang, Z.-F. Sun, D.-Y. Chen, X. Liu, T. Matsuki, Phys. Rev. D **85**, 074024 (2012). arXiv:1202.4139 [hep-ph]
29. Y. Sun, X. Liu, T. Matsuki, Phys. Rev. D **88**, 094020 (2013). arXiv:1309.2203 [hep-ph]
30. L.-P. He, X. Wang, X. Liu, Phys. Rev. D **88**, 034008 (2013). arXiv:1306.5562 [hep-ph]
31. Y. Sun, Q.-T. Song, D.-Y. Chen, X. Liu, S.-L. Zhu, Phys. Rev. D **89**, 054026 (2014). arXiv:1401.1595 [hep-ph]
32. C.-Q. Pang, L.-P. He, X. Liu, T. Matsuki, Phys. Rev. D **90**, 014001 (2014). arXiv:1405.3189 [hep-ph]
33. B. Wang, C.-Q. Pang, X. Liu, T. Matsuki, Phys. Rev. D **91**, 014025 (2015). arXiv:1410.3930 [hep-ph]
34. K. Chen, C.-Q. Pang, X. Liu, T. Matsuki, Phys. Rev. D **91**, 074025 (2015). arXiv:1501.07766 [hep-ph]
35. C. Langand, C. Rebbi, Phys. Lett. B **115**, 137 (1982)
36. S. Booth, D. Henty, A. Hulsebos, A. Irving, C. Michael, P. Stephenson, U. Collaboration et al., Phys. Lett. B **294**, 385 (1992)
37. G.S. Bali, Phys. Rept. **343**, 1 (2001)
38. T. Kawanaiand, S. Sasaki, Phy. Rev. Lett **107**, 091601 (2011)
39. T. Kawanaiand, S. Sasaki, Prog. Part. Nuclear Phys. **67**, 130 (2012)
40. W. Lucha, F.F. Schoberl, D. Gromes, Phys. Rept. **200**, 127 (1991)
41. A. Le Yaouanc, L. Oliver, O. Pene, J.-C. Raynal, Phys. Rev. D **9**, 1415 (1974)
42. A. Le Yaouanc, L. Oliver, O. Pene, J. Raynal, Phys. Rev. D **11**, 1272 (1975)
43. A. Le Yaouanc, L. Oliver, O. Pene, J. Raynal, Phys. Lett. B **72**, 57 (1977a)
44. A. Le Yaouanc, L. Oliver, O. Pene, J.-C. Raynal, Phys. Lett. B **71**, 397 (1977b)
45. P.R. Page, Nucl. Phys. B. **446**, 189 (1995). arXiv:hep-ph/9502204 [hep-ph]
46. A.I. Titov, T.I. Gulamov, B. Kampfer, Phys. Rev. D **53**, 3770 (1996)
47. H.G. Blundell. arXiv:hep-ph/9608473 (1996)
48. H.Q. Zhou, R.G. Ping, B.S. Zou, Phys. Lett. B **611**, 123 (2005). arXiv:hep-ph/0412221 [hep-ph]
49. Z.-G. Luo, X.-L. Chen, X. Liu, Phys. Rev. D **79**, 074020 (2009). arXiv:0901.0505 [hep-ph]
50. M. Jacoband, G. Wick, Ann. Phys. **7**, 404 (1959)
51. B.-Q. Liand, K.-T. Chao, Commun. Theor. Phys. **52**, 653 (2009a). arXiv:0909.1369 [hep-ph]
52. B.-Q. Liand, K.-T. Chao, Phys. Rev. D **79**, 094004 (2009b). arXiv:0903.5506 [hep-ph]
53. T. Matsuki, T. Morii, K. Seo, Prog. Theor. Phys. **124**, 285 (2010). arXiv:1001.4248 [hep-ph]
54. G.D. Tikhomirov, I.A. Erofeev, O.N. Erofeeva, V.N. Luzin, Phys. Atom. Nucl. **66**, 828 (2003) [**Yad. Fiz. 66, 860 (2003)**]
55. C. Daum et al., ACCMOR. Nucl. Phys. B **187**, 1 (1981)
56. G.W. Brandenburg, R.K. Carnegie, R.J. Cashmore, M. Davier, W.M. Dunwoodie, T.A. Lasinski, D.W.G.S. Leith, J.A.J. Matthews, P. Walden, S.H. Williams, Phys. Rev. Lett. **36**, 1239 (1976)
57. R. Aaij et al., LHCb. Phys. Rev. D **93**, 052018 (2016). arXiv:1509.06628 [hep-ex]
58. D. Aston et al., Nucl. Phys. B **296**, 493 (1988a)
59. D. Antreasyan et al., Crystal Ball. Z. Phys. C **48**, 561 (1990)
60. R.K. Carnegie, R.J. Cashmore, M. Davier, W.M. Dunwoodie, T.A. Lasinski, D.W.G.S. Leith, S.H. Williams, Nucl. Phys. B **127**, 509 (1977)
61. H.-Y. Cheng, C.-K. Chua, C.-W. Hwang, Phys. Rev. D **69**, 074025 (2004). arXiv:hep-ph/0310359 [hep-ph]
62. D.-M. Liand, Z. Li, Eur. Phys. J. A **28**, 369 (2006). arXiv:hep-ph/0606297 [hep-ph]
63. A. Tayduganov, E. Kou, A. Le Yaouanc, Phys. Rev. D **85**, 074011 (2012). arXiv:1111.6307 [hep-ph]
64. D. Aston et al., Nucl. Phys. B **292**, 693 (1987)
65. D. Frame, I.S. Hughes, J.G. Lynch, P.W. Minto, D.M. McFadzean, D.T. Stewart, A.S. Thompson, R.M. Turnbull, I.T. Wilkie, Nucl. Phys. B **276**, 667 (1986)
66. R. Aaij et al., LHCb. Phys. Rev. Lett. **118**, 022003 (2017). arXiv:1606.07895 [hep-ex]
67. T. Armstrong et al., Bari-Birmingham-CERN-Milan-Paris-Pavia. Nucl. Phys. B **221**, 1 (1983a)
68. H.-Y. Cheng, Phys. Lett. B **707**, 116 (2012). arXiv:1110.2249 [hep-ph]
69. A. Firestone, G. Goldhaber, D. Lissauer, G.H. Trilling, Phys. Rev. D **5**, 505 (1972)
70. M. Baubillier et al., Birmingham-CERN-Glasgow-Michigan State-Paris. Z. Phys. C **26**, 37 (1984)
71. D. Aston et al., Phys. Lett. B **149**, 258 (1984)
72. D. Aston et al., Phys. Lett. B **201**, 169 (1988b)
73. D. Aston et al., Phys. Lett. B **99**, 502 (1981)
74. D. Aston et al., Phys. Lett. B **180**, 308 (1986) [**Erratum: Phys. Lett. B 183, 434 (1987)**]
75. T. Armstrong et al., Bari-Birmingham-CERN-Milan-Paris-Pavia. Nucl. Phys. B **227**, 365 (1983b)
76. W.E. Cleland et al., Nucl. Phys. B **184**, 1 (1981)
77. R. Aaij et al., LHCb. Phys. Rev. Lett. **115**, 072001 (2015). arXiv:1507.03414 [hep-ex]